CalVal Jason-2

Jason-2 validation and cross calibration activities

Contract No 60453/00 - lot2.C

Reference : CLS.DOS/NT/09-007

Nomenclature : SALP-RP-MA-EA-21632-CLS

Issue : 1rev 1

Date : May 15, 2009

SALP Service Altimetrie & Localisation Precise

CLS Collecte Localisation Satellites

cnes Centre National d'Études Spatiales

CLS - 8-10 Rue Hermès - Parc Technologique du Canal - 31520 Ramonville St-Agne - FRANCE
Telephone 33 5 61 39 47 00 / Fax 33 5 61 75 10 14

Chronology Issues:		
Issue:	Date:	Reason for change:
1rev0	January 29, 2009	Creation
1rev1	May 15, 2009	Revision after comments from N. Picot

People involved in this issue:		
Written by:	S. Philipps M. Ablain	CLS CLS
Checked by:	DT/AQM	CLS
Approved by:	JP. Dumont	CLS
Application authorized by:		

Index Sheet :	
Context:	
Keywords:	
Hyperlink:	

Distribution:		
Company	Means of distribution	Names
CLS/DOS	1 electronic copy	G.DIBARBOURE
	1 electronic copy	V.ROSMORDUC
	1 electronic copy	P.ESCUDIER
	1 electronic copy	J.DORANDEU
DOC/CLS	1 electronic copy	DOCUMENTATION
CNES	1 cd-rom	T.GUINLE
CNES	1 cd-rom	P.BOUBE
CNES	1 cd-rom	D.CHERMAIN
CNES	1 electronic copy	E.BRONNER
CNES	1 electronic copy	J.LAMBIN
CNES	1 electronic copy	A.LOMBARD
CNES	1 electronic copy	N.PICOT

List of tables and figures

List of Tables

List of Figures

List of items to be defined or to be confirmed

Applicable documents / reference documents

Contents

1. Introduction

This document presents the synthesis report concerning validation activities of Jason-2 IGDRs under SALP contract (N° 60453/00 Lot2.C) supported by CNES at the CLS Space Oceanography Division. It is divided into two parts: CAL/VAL Jason-2 activities - Jason-2 / Jason-1 cross-calibration.

The OSTM/Jason-2 satellite was successfully launched on June, 20th 2008. Since July, 4th, Jason-2 is on its final orbit. Until January 2009, it was flying in tandem with Jason-1, only 55s apart. Since the beginning of the mission, Jason-2 data have been analyzed and monitored in order to assess the quality of Jason-2 products. Cycle per cycle reports are available on the Jason-2 project server.

This present report assesses the Jason-2 data quality. Missing and edited measurements are monitored. Furthermore relevant parameters derived from instrumental measurements and geophysical corrections are analyzed.

Analyzes are focused on Jason-1/Jason-2 cross-calibration since both missions were on the same orbit during the Calibration/Validation phase until the 26th of January 2009. This allows to precisely assess parameter discrepancies between both missions in order to detect geographically correlated biases, jumps or drifts. The SLA performances and consistency with Jason-1 are also described. Even if only low order statistics are mainly presented here, other analyzes including histograms, plots and maps are continuously produced and used in the quality assessment process. Indeed, it is now well recognized that the usefulness of any altimeter data only makes sense in a multi-mission context, given the growing importance of scientific needs and applications, in particular for operational oceanography. One major objective of the Jason-2 mission is to continue the Jason-1 and T/P high precision altimetry and to allow combination with other missions (ENVISAT, Jason-1). This kind of comparisons between different altimeter missions flying together provides a large number of estimations and consequently efficient long term monitoring of instrument measurements.

2. Processing status

2.1. Processing

End of 2008 Jason-2 data were already available to end users in OGDR (3h data latency) and IGDR (1-2 days data latency). They are available in version "c", the same version as Jason-1 data (for better compatibility). GDR data were not available, but POE (precise orbit ephemeris) were already produced for several cycles. In this report, IGDRs from cycle 0 to 17 are used (till 27/12/2008). But results using OGDRs or POEs are also presented. A description of the different Jason-2 products is available in the OSTM/Jason-2 Products handbook ([5]).
The purpose of this document is to report the major features of the data quality from the Jason-2 mission. As Jason-2 was in tandem flight formation with Jason-1 (only 55 s apart) till January 2009, this report focuses on intercalibration with Jason-1.

2.2. CAL/VAL status

2.2.1. List of events

The following table shows the major plannified events during the beginning of Jason-2 mission.

Dates	Events	Impacts
4 July 2008 5h57	Start of Jason-2 Cycle 0	
4 July 2008 12h15	Start of Poseidon3 altimeter. Tracking mode : autonomous acquisition, median	Start of level2 product generation.
04 July 2008 13:47:52 to 04 July 2008 14:13:36	Poseidon3 altimeter. Tracking mode : Diode acquisition, median	
04 July 2008 14:14:39 to 17 July 2008 15:30:22	Poseidon3 altimeter. Tracking mode : Diode acquisition, SGT	
8 July 2008 4h45 - 5h25	Poseidon3 altimeter. Dedicated period for validation of tracking mode performances	small data gaps on corresponding passes [Cycle 0]
11 July 2008 13h00-13h01 and 13h04-13h12	Poseidon3 altimeter. Tracking mode : Diode-DEM (functional)	Functional test of DIODE-DEM tracking mode while onboard DEM was not correct, leading to wrong waveforms and so impacts on altimeter retracking outputs.
		.../...

Dates	Events	Impacts
12 July 2008 1h20	Start of Jason-2 Cycle 1	
16 July 2008 7h10-17h08	upload POS3 - DEM	Data gap on corresponding passes [Cycle 1, Pass 108-144]
17 July 2008 7h29-11h30	upload POS3 - DEM	Data gap on corresponding passes [Cycle 1, Pass 108-144]
17 July 2008 15:30:22 to 31 July 2008 21:17:08 UTC	Poseidon3 altimeter. Tracking mode : Diode acquisition, median	
21 July 2008 23h18	Start of Jason-2 Cycle 2	
31 July 2008 21:17:09 to 10 August 2008 19:15:39	Jason-2 Cycle 3: Poseidon3 altimeter. Tracking mode : Diode-DEM	
10 August 2008 19:15:40 to 20 August 2008 17:14:10	Jason-2 Cycle 4: Poseidon3 altimeter. Tracking mode : Diode acquisition, median	
20 August 2008 17:14:11 to 30 August 2008 15:12:43	Jason-2 Cycle 5: Poseidon3 altimeter. Tracking mode : Diode-DEM	
30 August 2008 15:12:43 to 9 September 2008 13:11:15	Jason-2 Cycle 6: Poseidon3 altimeter. Tracking mode : Diode acquisition, median	
9 September 2008 13:11:15 to 19 September 2008 11:09:47	Jason-2 Cycle 7: Poseidon3 altimeter. Tracking mode : Diode-DEM	
19 September 2008 11:09:47 to 29 September 2008 09:08:19	Jason-2 Cycle 8: Poseidon3 altimeter. Tracking mode : Diode acquisition, median	

Table 1: *P*lannified events

2.2.2. Missing measurements

This section presents a summary of major satellite or ground segment events that occurred from cycle 0 to 17. Table 2 gives a status about the number of missing passes (or partly missing) for IGDRs and OGDRs, as well as the associated events for each cycle.
During its first months, Jason-2 has little missing measurements. They were mainly caused by station acquisition problems or ground processing anomalies.

Jason-2 Cycles/Pass	Dates	Events	IGDR	OGDR
000/222-224	10/07/08 - 18:28:02 to 20:25:04	Missing telemetry (Usingen station pb)	x	x
000/232	11/07/08 - 03:57:08 to 04:30:30	Partly missing due to altimeter calibration (long LPF)	x	x
000/235	11/07/08 - 07:01:28 to 07:27:41	Partly missing due to altimeter calibration (CNG step)	x	x
001/44-46	13/07/08 - 17:40:00 to 19:37:30	Missing telemetry (Usingen station pb)	x	x
001/48-50	13/07/08 - 21:37:02 to 23:30:00	Missing telemetry (NOAA station pb)	x	x
001/102	15/07/08 - 23:57:45 to 16/07/08 00:54:00	Processing anomaly	x	-
001/108-144		several passes partly missing due to upload of new DEM (plannified unavailability)	x	x
001/145	17/07/08 - 16:14:59 to 17:11:12	Processing anomaly (wrong management of telemetry sequence count) on CNES side	x	-
003/032-035	02/08/08 - 02:23:45 to 05:46:30	Passes 32 and 35 are partly missing, passes 33 and 34 are completely missing due to missing telemetry (Usingen)	x	x
005/141	26/08/08 - 04:24:15 to 05:20:27	Processing anomaly	x	-
005/236-241	29/08/08 - 21:44:56 to 30/08/2008 02:52:07	Missing telemetry (Usingen station pb): passes 237 to 240 completely missing, passes 236 and 241 partly missing	x	x
006/232	08/09/08 - 15:48:00 to 16:21:22	pass 232 partially missing due to altimeter calibration (long LPF)	x	x
006/235	08/09/08 - 18:53:00 to 19:19:10	pass 235 partially missing due to altimeter calibration (CNG step)	x	x
016/73	10/12/08 - 15:11:19 to 15:13:27	pass 73 partially missing due to 1) upload of correction for low signal tracking anomaly and 2) memory dumps (planned unavailability)	x	x

.../...

Jason-2 Cycles/Pass	Dates	Events	IGDR	OGDR

Table 2: *M*issing pass status

2.2.3. Edited measurements

Table 3 indicates particular high editing periods (see section 3.2.1.). Most of the occurrences correspond to radiometer wet troposphere correction at default value (due to processing anomalies) or altimeter low signal tracking anomaly (AGC anomaly), though the latter concerns only few measurements and was corrected during cycle 16 (see section 7.1.).

Jason-2 Cycles/Passes	Date	Comments	IGD	OGDR
000/71-73	04/07/08 - 20:56:35 to 23:45:12	Completely edited by SLA out of threshold (related to maneuver at 22:31:58)	-	x
000/75	05/07/08 - 01:26:02 to 01:37:38	Partly edited by SLA out of threshold (related to maneuver at 01:20:37)	-	x
000/89	05/07/08 - 14:22:07 to 14:23:38	Partly edited by several parameters out of threshold (AGC anomaly)	x	x
000/134	07/07/08 - 08:06:37 to 08:28:57	Partly edited by several parameters out of threshold (AGC anomaly)	x	x
000/156	08/07/08 - 04:35:12 to 05:31:01	rain flag is set (dotted), probably related to start/stop sequence (from 04:45 to 05:24)	x	x
000/234	11/07/08 - 05:45:12 to 05:49:03	Partly edited by several parameters out of threshold (AGC anomaly)	x	x
000/241	11/07/08 - 13:04:27 to 13:09:11	Partly edited by ice flag (number of elementary Ku-band measurements at 0, AGC=16.88) due to test of altimeter DEM mode	x	x
001/		several passes partly edited by several parameters out of threshold (AGC anomaly)	x	x
002/		several passes partly edited by several parameters out of threshold (AGC anomaly)	x	x
				.../...

Jason-2 Cycles/Passes	Date	Comments	IGD	OGDR
002/33-35	23/07/08 - 05:54:19 to 07:48:41	Pass 034 completely, as well as passes 033 and 035 partly edited by wet troposphere radiometer correction at default value due to processing anomaly. Related to a ground processing anomaly on one radiometer telemetry file.	x	-
002/72	24/07/08 - 17:53:16 to 18:09:44	Pass 072 partly edited by wet troposphere radiometer correction at default value. Related to a ground processing anomaly and several telemetry segments with overlaps.	x	-
004/		several passes partly edited by several parameters out of threshold (AGC anomaly)	x	x
004/010	11/08/08 - 04:01:29 to 04:05:52	Ogdr :Pass 010 partly edited by radiometer wet troposphere correction at default value	-	x
004/246	20/08/2008 - 08:48:15 to 09:44:28	Ogdr: Completely edited by statistics on SLA (std of SLA on pass 246 higher than 0.3 m), probably due to bad orbit quality due to yaw flip	-	x
005/139,140	26/08/2008 - approx. 03:17:34 to 04:24:14	radiometer wet troposphere correction at default value for a portion of pass 139 and almost for all pass 140 (processing anomaly)	x	-
009/067	01/10/2008 - 23:16:44 to 23:21:07	Pass 067 partly edited in Ogdr by radiometer wet troposphere correction at default value	-	x
017/034	18/12/2008 - 23:51:39 to 19/12/2008 00:47:48	Pass 034 completely edited in Ogdr by statistics on SLA (probably related to maneuver burn during pass 33)	-	x

Table 3: *E*dited measurement status

2.3. Models and Standards History

Two versions of the Jason-2 Operational Geophysical Data Records (OGDRs) and Interim Geophysical Data Records (IGDRs) have been generated to date. These two versions are identified by the version numbers "T" (for test) and "c" in the product filename. For example, version "T" IGDRs are named "JA2_IPN_2PT" and version "c" IGDRs are named "JA2_IPN_2Pc". Both versions adopt an identical data record format as described in Jason-2 User Handbook ([5]) and differ only sligthly (names of variables are corrected and 3 variables added). Version "T" O/IGDRs were the first version released soon after launch and was disseminated only to OSTST community. Version "c" O/IGDRs were first implemented operationally from data segment 141 of cycle 15 for the OGDRs (3rd December 2008) and cycle 15 for the IGDRs. Version "c" of Jason-2 data is consistent with version "c" of Jason-1 data. The table 4 below summarizes the models and standards that are adopted for Jason O/IGDRs. More details on some of these models are provided in Jason-2 User Handbook document ([5]).

Model	OGDR	IGDR
Orbit	DORIS Navigator	Preliminary DORIS
Altimeter (Ocean) Retracking	MLE4 fit from 2nd order Brown model: MLE4 simultaneously retrieves the 4 parameters that can be inverted from the altimeter waveforms: epoch, SWH, Sigma0 and mispointing angle	MLE4 fit from 2nd order Brown model: MLE4 simultaneously retrieves the 4 parameters that can be inverted from the altimeter waveforms: epoch, SWH, Sigma0 and mispointing angle
Altimeter Instrument Corrections	Consistent with MLE4 retracking algorithm.	Consistent with MLE4 retracking algorithm.
Jason-2 Advanced Microwave Radiometer (AMR) Parameters	Using calibration parameters derived from long term calibration tool developed and operated by NASA/JPL, knowing that the 1st update of the AMR calibration was performed early 2009	Using calibration parameters derived from long term calibration tool developed and operated by NASA/JPL, knowing that the 1st update of the AMR calibration was performed early 2009 .
Dry Troposphere Range Correction	From ECMWF atmospheric pressures and model for S1 and S2 atmospheric tides	From ECMWF atmospheric pressures and model for S1 and S2 atmospheric tides.
Wet Troposphere Range Correction from Model	From ECMWF model	From ECMWF model.
		.../...

Model	OGDR	IGDR
Sea State Bias Model	Empirical model derived from 3 years of MLE4 Jason-1 altimeter data with version "b" geophysical models.	Empirical model derived from 3 years of MLE4 Jason-1 altimeter data with version "b" geophysical models.
Mean Sea Surface Model	CLS01	CLS01
Geoid	EGM96	EGM96
Bathymetry Model	DTM2000.1	DTM2000.1
Inverse Barometer Correction	Computed from ECMWF atmospheric pressures after removing S1 and S2 atmospheric tides	Computed from ECMWF atmospheric pressures after removing S1 and S2 atmospheric tides.
Non-tidal High-frequency Dealiasing Correction	None (set to default)	Mog2D high resolution ocean model on I/GDRs. Ocean model forced by ECMWF atmospheric pressures after removing S1 and S2 atmospheric tides.
Tide Solution 1	GOT00.2 + S1 ocean tide . S1 load tide ignored	GOT00.2 + S1 ocean tide . S1 load tide ignored.
Tide Solution 2	FES2004 + S1 and M4 ocean tides. S1 and M4 load tides ignored	FES2004 + S1 and M4 ocean tides. S1 and M4 load tides ignored.
Equilibrium long-period ocean tide model.	From Cartwright and Taylor tidal potential.	From Cartwright and Taylor tidal potential.
Non-equilibrium long-period ocean tide model.	Mm, Mf, Mtm, and Msqm from FES2004	Mm, Mf, Mtm, and Msqm from FES2004.
Solid Earth Tide Model	From Cartwright and Taylor tidal potential.	From Cartwright and Taylor tidal potential.
Pole Tide Model	Equilibrium model	Equilibrium model.
Wind Speed from Model	ECMWF model	ECMWF model
Altimeter Wind Speed	Table derived from version "a" Jason-1 GDR data.	Table derived from version "a" Jason-1 GDR data.

Table 4: *M*odels and standards adopted for the Jason-2 OGDR and IGDR products

3. Data coverage and edited measurements

3.1. Missing measurements

3.1.1. Over ocean

Determination of missing measurements relative to the theoretically expected orbit ground pattern is used to detect missing telemetry in Jason-2 datasets due to altimetry events for instance. This procedure is applied cycle per cycle and leads to results plotted on the left figure 1. It represents the percentage of missing measurements relative to the theory, when limited to ocean surfaces. The mean value is about 2.0% but this figure is not significant due to several events where the measurements are missing (as for example cycle 0 has only 8 days instead of 10). All these events are described on table 2.
On figure 1 on the right, the percentage of missing measurements is plotted without taking into account the cycles where instrumental events or other anomalies occurred. Moreover shallow waters and high latitudes have been removed. This allows us to detect small data gaps in open ocean. The mean value is about 0.01%. This weak percentage of missing measurements is mainly explained by the rain cells and sigma0 blooms. These sea states can disturb significantly the Ku band waveform shape leading to an altimeter lost of tracking. Discontinuities at the border between the reception stations (NOAA and Usingen) may also lead to missing measurements.

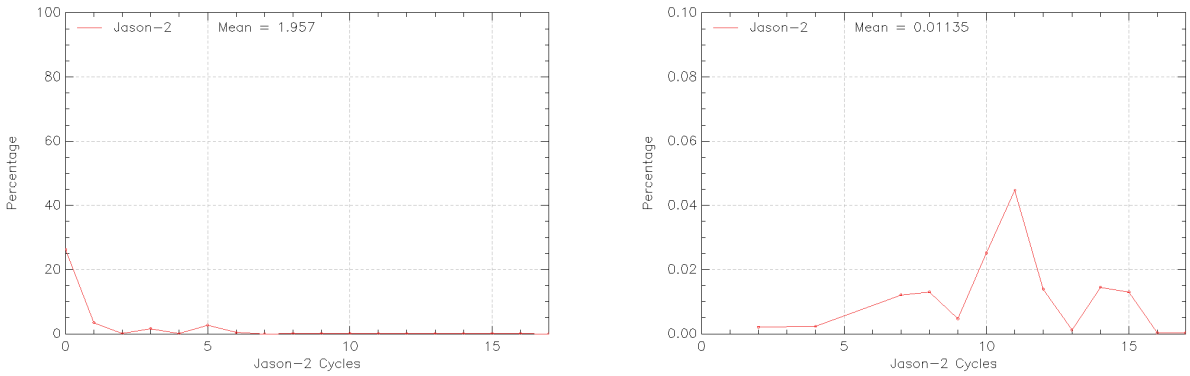

Figure 1: *Cycle per cycle percentage of missing measurements over ocean*

3.1.2. Over land and ocean

Figure 2 shows the percentage of missing measurements for Jason-2 and Jason-1 (all surfaces) computed with respect to a theoretical possible number of measurements. Due to differences between altimeter tracking algorithms, the number of data is greater for Jason-2 than for Jason-1. Differences appear on land surfaces as shown in figure 3. Since cycle 16, percentage of missing measurements of Jason-2 has slightly increased due to the correction of the low signal tracking anomaly (see section 7.1.). The missing data are highly correlated with the mountains location.

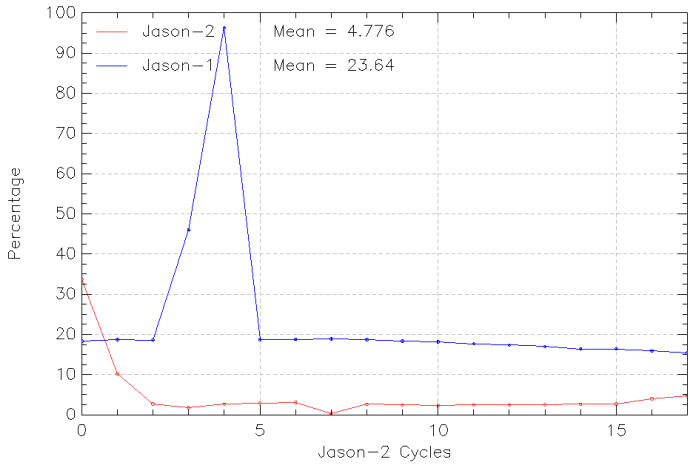

Figure 2: *Percentage of missing measurements over ocean and land for JA2 and JA1*

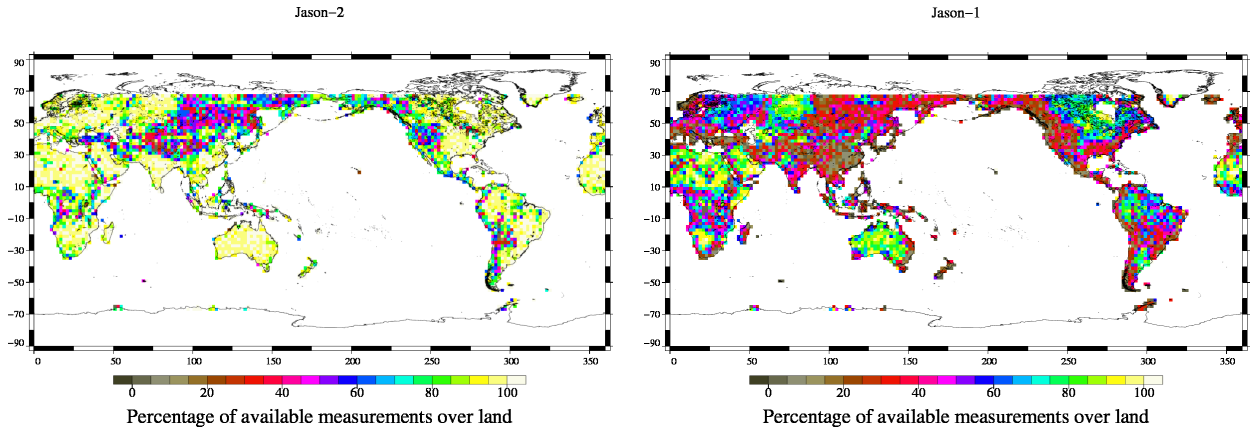

Figure 3: *Map of percentage of available measurements over land for Jason-2 on cycle 17 (left) and for Jason-1 on cycle 256 (right)*

3.2. Edited measurements

3.2.1. Editing criteria definition

Editing criteria are used to select valid measurements over ocean. The editing process is divided into 4 parts. First, only measurements over ocean and lakes are kept (see section 3.2.2.). Second, some flags are used as described in section 3.2.3. and 3.2.4.. Then, threshold criteria are applied on altimeter, radiometer and geophysical parameters and are described in the table 5. Moreover, a spline criterion is applied to remove the remaining spurious data. For each criterion, the cycle per cycle percentage of edited measurements has been monitored. This allows detection of anomalies in the number of removed data, which could come from instrumental, geophysical or algorithmic changes.

Parameter	Min thresholds	Max thresholds	mean edited
Sea surface height	$-130\,m$	$100\,m$	0.28%
Sea level anomaly	$-10\,m$	$10.0\,m$	0.69%
Number measurements of range	10	*Not applicable*	0.38%
Standard deviation of range	0	$0.2\,m$	1.48%
Squared off-nadir angle	$-0.2\,deg^2$	$0.64\,deg^2$	0.83%
Dry troposphere correction	$-2.5\,m$	$-1.9\,m$	0.00%
Inverted barometer correction	$-2.0\,m$	$2.0\,m$	0.00%
AMR wet troposphere correction	$-0.5m$	$-0.001\,m$	0.14%
Ionosphere correction	$-0.4\,m$	$0.04\,m$	1.08%
Significant wave height	$0.0\,m$	$11.0\,m$	0.49%
Sea State Bias	$-0.5\,m$	$0.0\,m$	0.18%
Number measurements of Ku-band Sigma0	10	*Not applicable*	0.37%
Standard deviation of Ku-band Sigma0	0	$1.0\,dB$	2.39%
Ku-band Sigma0 [1]	$7.0\,dB$	$30.0\,dB$	0.35%
Ocean tide	$-5.0\,m$	$5.0\,m$	0.07%
Equilibrium tide	$-0.5\,m$	$0.5\,m$	0.00%
Earth tide	$-1.0\,m$	$1.0\,m$	0.00%
Pole tide	$-15.0\,m$	$15.0\,m$	0.00%

.../...

Parameter	Min thresholds	Max thresholds	mean edited
Altimeter wind speed	$0\,m.s^{-1}$	$30.0\,m.s^{-1}$	0.65%
All together	-	-	3.6%

Table 5: *E*diting criteria

3.2.2. Selection of measurements over ocean and lakes

In order to remove data over land, a land-water mask is used. Only measurements over ocean or lakes are kept. This allows to keep data near the coasts and so to detect potential anomalies in these areas. Furthermore, there is no impact on global performance estimations since the most significant results are derived from analyzes in deep ocean areas. Figure 4 shows the cycle per cycle percentage of measurements eliminated by this selection. The signal reflects the impact of the different altimeter tracking modes: SGT (split gate tracking), Median and DIODE/DEM (digital elevation model). SGT mode, the nominal mode for Jason-1, was used for Jason-2 during cycle 0 and half of cycle 1. This mode does not perform very well over land (as also depicted on right side of figure 3), therefore a comparable small percentage of measurements are edited over land for cycles 0 and 1 (approximately 21%). Most of Jason-2 cycles (cycles 2, 4, 6, and onwards from cycle 8) were operated in Median mode (also used by Envisat). This mode is more adapted for tracking over land than SGT and provides therefore more measurements over land (as also seen on left side of figure 3) and so more measurements are edited (approximately 27%) due to the ocean/land criteria. A new tracking mode, DEM, was used during cycles 3, 5, and 7. It has been designed to provide more data over inland water surfaces and coastal areas. It provides a continuous data set over land but some are not meaningful (in areas where the DEM is not accurate enough like in the major mountains). Therefore during these cycles, almost 29% of measurements are removed by the selection. Since 10th of December, 2008 the onbord altimeter configuration was modified to correct for the low signal tracking anomaly, which led to a more strict control of acquisition gain loop (to avoid the tracking of low signal anomalies). This explains the small decrease of land measurements edited for cycles 16 onwards (section 7.1.).

[1]The thresholds used for the Ku-band Sigma0 are the same than for Jason-1 and T/P, but the same sigma0 bias as between Jason-1 and T/P (about 2.4 dB) is applied.

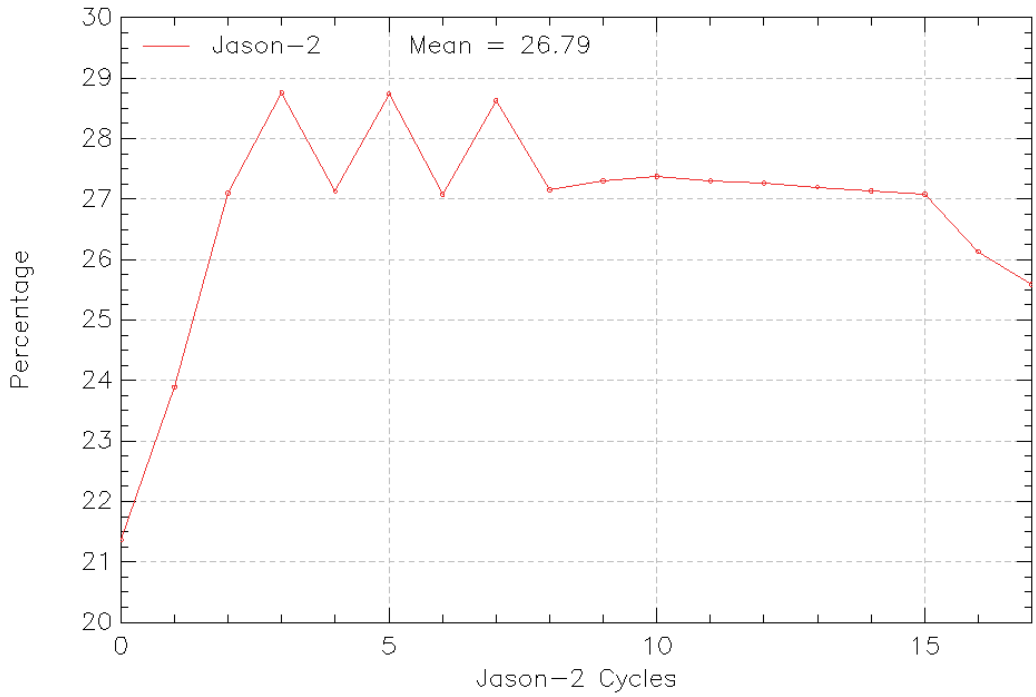

Figure 4: *Cycle per cycle percentage of eliminated measurements during selection of ocean/lake measurements.*

3.2.3. Flagging quality criteria: Ice flag

The ice flag is used to remove the sea ice data. Figure 5 shows the cycle per cycle percentage of measurements edited by this criterion. Over that short period, no anomalous trend is detected (figure 5 left) but a start of the nominal annual cycle is visible. Indeed, the maximum number of points over ice is reached during the southern winter (ie. July - September). As Jason-2 takes measurements between 66° north and south, it does not detect thawing of sea ice (due to global warming), which takes place especially in northern hemisphere over 66°N. The percentage of measurements edited by ice flag is plotted in the right of figure 5 for a period of 6 month.

3.2.4. Flagging quality criteria: Rain flag

The rain flag is not used for data selection since it is not yet tuned for Jason-2, as easily visible on figure 6 showing the percentage of rain edited measurements over cycles 0 to 17 (covering almost 6 months). Only measurements near coasts and passes with radiometer wet troposphere correction at default value are flagged as rain. The few passes in yellow visible in figure 6 are linked to radiometer processing anomalies. Indeed rain flag was tuned on Jason-1 automatic gain control loop measurements. As automatic gain control loop is different for Jason-2 and Jason-1 the rain flag currently does not work. It is thus recommended to not use this flag.

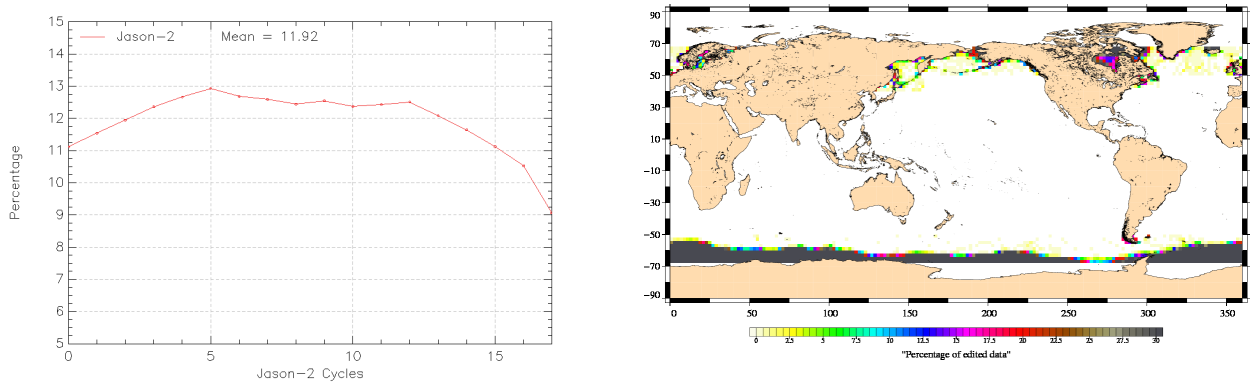

Figure 5: *Percentage of edited measurements by ice flag criterion. Left: Cycle per cycle monitoring. Right: Map over a sixth month period (cycles 0 to 17).*

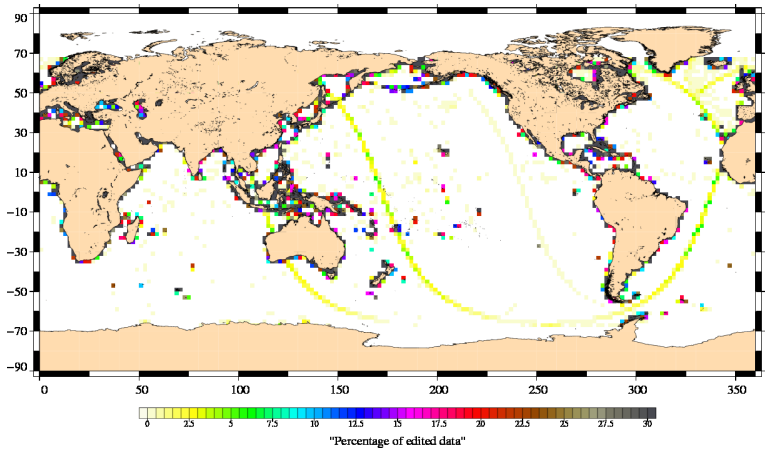

Figure 6: *Map of percentage of edited measurements by rain flag criterion over sixth month period (cycles 0 to 17).*

3.2.5. Threshold criteria: Global

Instrumental parameters have also been analyzed from comparison with thresholds, after having selected only ocean/lakes measurements and applied flagging quality criteria (ice flag). Note that no measurement is edited by the following corrections : dry troposphere correction, inverted barometer correction (including DAC), equilibrium tide, earth and pole tide. Indeed these parameters are only verified in order to detect data at default values, which might happen during a processing anomaly.
The percentage of measurements edited using each criterion is monitored on a cycle per cycle basis (figure 7). The mean percentage of edited measurements is about 3.6%. A slight decrease is visible, which is probably part of an annual cycle due to the seasonal sea ice coverage.

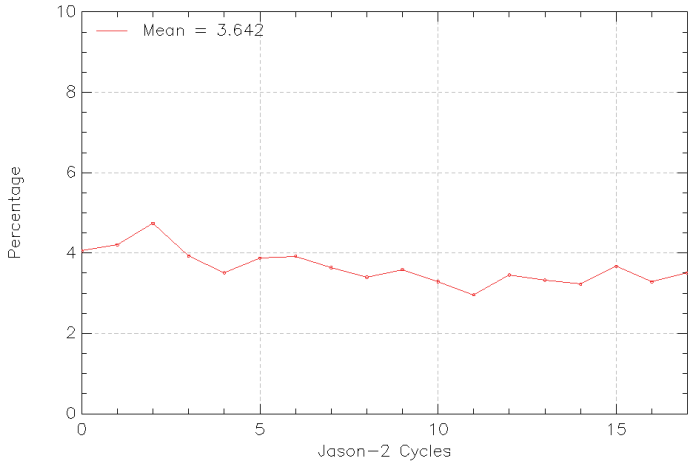

Figure 7: *Cycle per cycle percentage of edited measurements by threshold criteria*

3.2.6. Threshold criteria: 20-Hz measurements number

The percentage of edited measurements because of a too low number of 20-Hz measurements is represented on left side of figure 8. No trend neither any anomaly has been detected.
The map of measurements edited by 20-Hz measurements number criterion is plotted on right side of figure 8 and shows correlation with heavy rain and wet areas. Indeed waveforms are distorted by rain cells, which makes them often meaningless for SSH calculation. As a consequence, edited measurements due to several altimetric criteria are often correlated with wet areas.

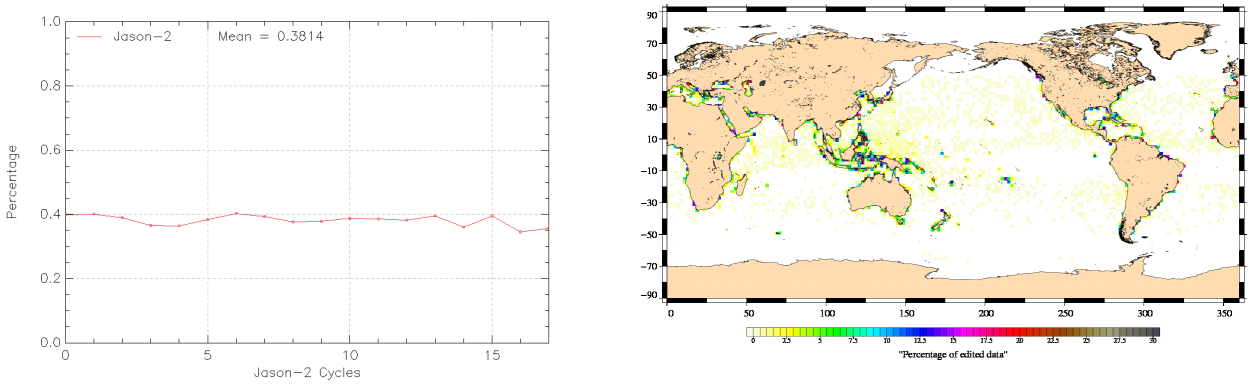

Figure 8: *Percentage of edited measurements by 20-Hz measurements number criterion. Left: Cycle per cycle monitoring. Right: Map over a sixth month period (cycles 0 to 17).*

3.2.7. Threshold criteria: 20-Hz measurements standard deviation

The percentage of edited measurements due to 20-Hz measurements standard deviation criterion is shown in figure 9 (left). During cycles 0 and 1, slightly more measurements are edited by 20-Hz measurements standard deviation criterion than during other cycles. This is likely due to low signal tracking anomaly which occurred during these cycles. These portions of passes are also visible on the right side of figure 9 showing a map of measurements edited by the 20-Hz measurements standard deviation criterion. As in section 3.2.6., edited measurements are correlated with wet areas, but also in regions where ice flag probably missed detection of sea ice (near Antarctic).

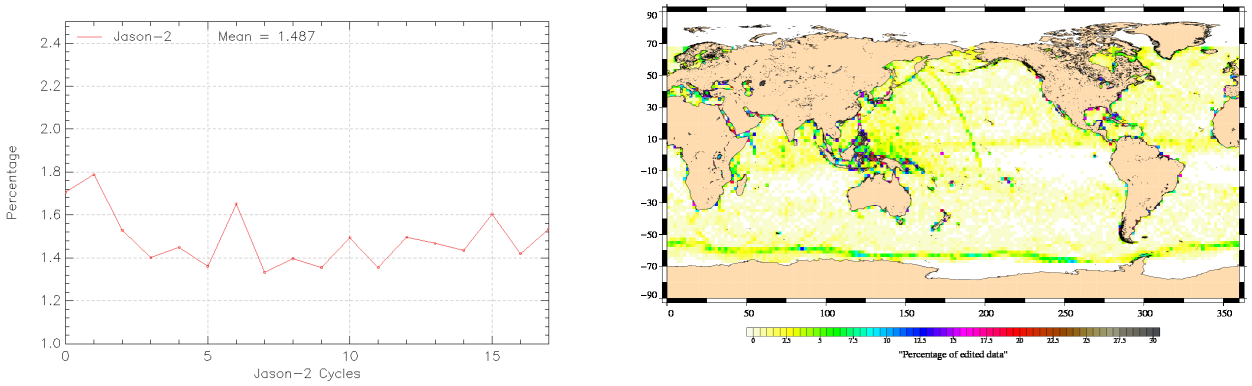

Figure 9: *Percentage of edited measurements by 20-Hz measurements standard deviation criterion. Left: Cycle per cycle monitoring. Right: Map over a sixth month period (cycles 0 to 17).*

3.2.8. Threshold criteria: Significant wave height

The percentage of edited measurements due to significant wave height criterion is represented in figure 10. It is about 0.50%. In the beginning of the mission, the curve of measurements edited by SWH threshold criterion is quite irregular, as low signal tracking anomalies occurred during SGT and Median tracking modes, whereas there are no low signal tracking anomalies during DEM tracking modes (cycles 3, 5, and 7). Indeed during periods of low signal tracking anomaly, parameters like significant wave height, backscattering coefficient and squared off-nadir angle from waveforms are out of thresholds and therefore edited (see section 7.1.). Figure 10 (right part) shows that measurements edited by SWH criterion are especially found near coasts in the equatorial regions.

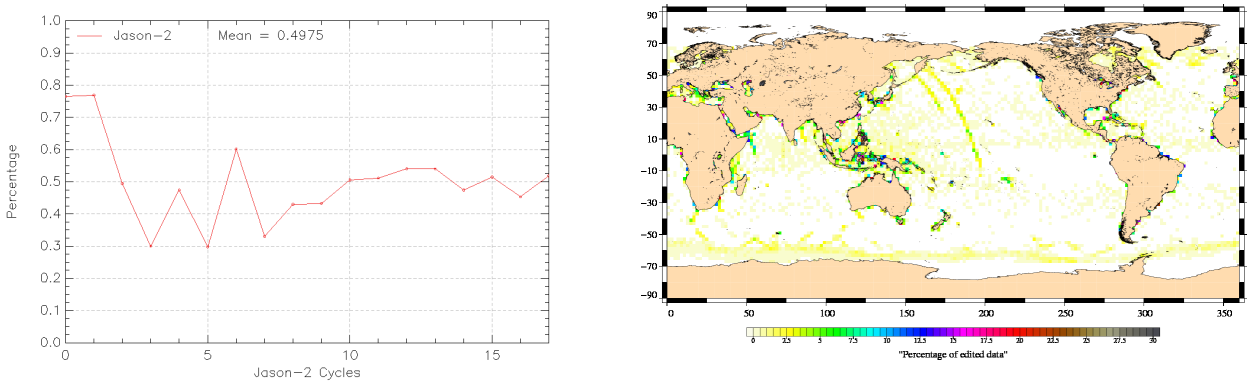

Figure 10: *Percentage of edited measurements by SWH criterion. Left: Cycle per cycle monitoring. Right: Map over a sixth month period (cycles 0 to 17).*

3.2.9. Backscatter coefficient

The percentage of edited measurements due to backscatter coefficient criterion is represented in figure 11. It is about 0.36% It is also impacted by low signal tracking anomalies, especially during cycles 0 and 1. The right part of figure 11 shows that measurements edited by backscatter coefficient criterion are especially found near coasts in the equatorial regions and closed sea (Mediterranean).

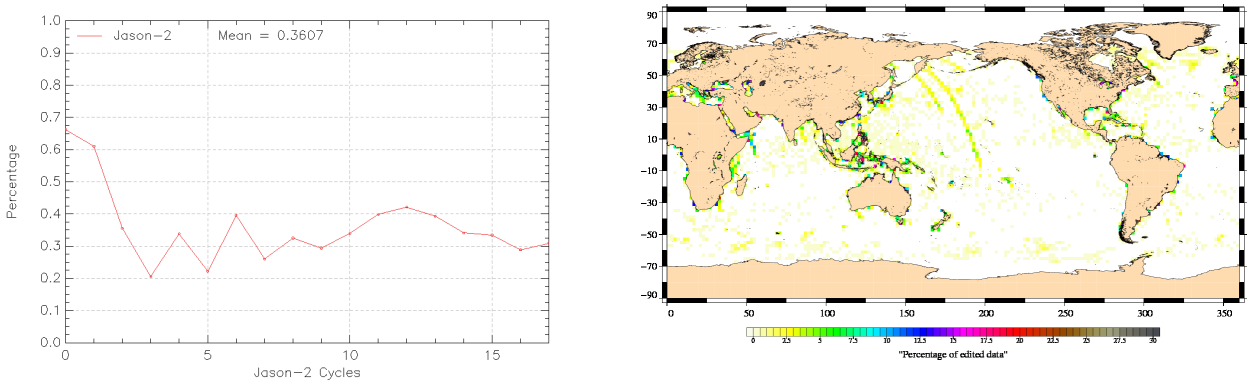

Figure 11: *Percentage of edited measurements by Sigma0 criterion. Left: Cycle per cycle monitoring. Right: Map over a sixth month period (cycles 0 to 17).*

3.2.10. Backscatter coefficient: 20 Hz standard deviation

The percentage of edited measurements due to 20 Hz backscatter coefficient standard deviation criterion is represented in figure 12. It is about 2.4%. It is also impacted by low signal tracking anomalies, especially during cycles 0 and 1. The right part of figure 11 shows that measurements edited by 20 Hz backscatter coefficient standard deviation criterion are especially found in regions with disturbed waveforms.

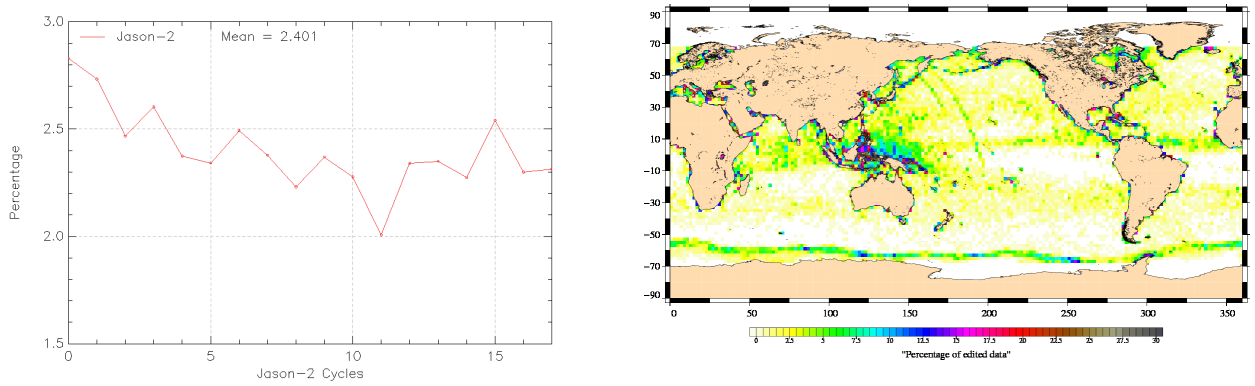

Figure 12: *Percentage of edited measurements by 20 Hz Sigma0 standard deviation criterion. Left: Cycle per cycle monitoring. Right: Map over a sixth month period (cycles 0 to 17).*

3.2.11. Radiometer wet troposphere correction

The percentage of edited measurements due to radiometer wet troposphere correction criterion is represented in figure 13. It is about 0.15%. When removing cycles which experienced problems, percentage of edited measurements drops to 0.07%. For cycles 2 and 5 the percentage of edited measurements is higher than usual. This is linked to radiometer wet troposphere correction at default value due to ground processing anomalies. Passes concerned are easily detectable on right side of figure 13.

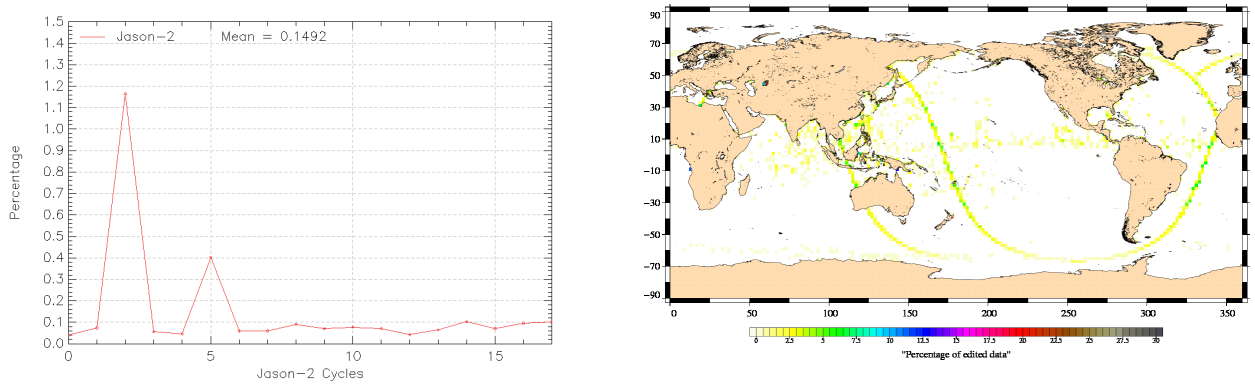

Figure 13: *Percentage of edited measurements by radiometer wet troposphere criterion. Left: Cycle per cycle monitoring. Right: Map over a sixth month period (cycles 0 to 17).*

3.2.12. Dual frequency ionosphere correction

The percentage of edited measurements due to dual frequency ionosphere correction criterion is represented in figure 14. It is about 1.08% and shows no drift. The map 14 shows that measurements edited by dual frequency ionosphere correction are mostly found in equatorial regions, but also near sea ice. Several pass-sections are visible. They were impacted by low signal tracking anomaly.

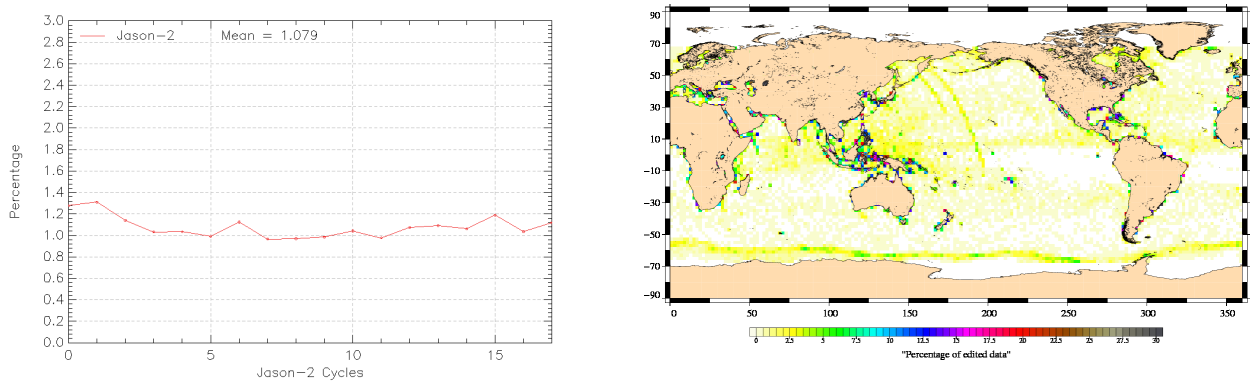

Figure 14: *Percentage of edited measurements by dual frequency ionosphere criterion. Left: Cycle per cycle monitoring. Right: Map over a sixth month period (cycles 0 to 17).*

3.2.13. Square off-nadir angle

The percentage of edited measurements due to square off-nadir angle criterion is represented in figure 15. It is about 0.83%. As for other parameters, impact of low signal tracking anomalies is visible especially for cycles 0 and 1. The map 15 shows that edited measurements are mostly found in coastal regions and regions with disturbed waveforms.

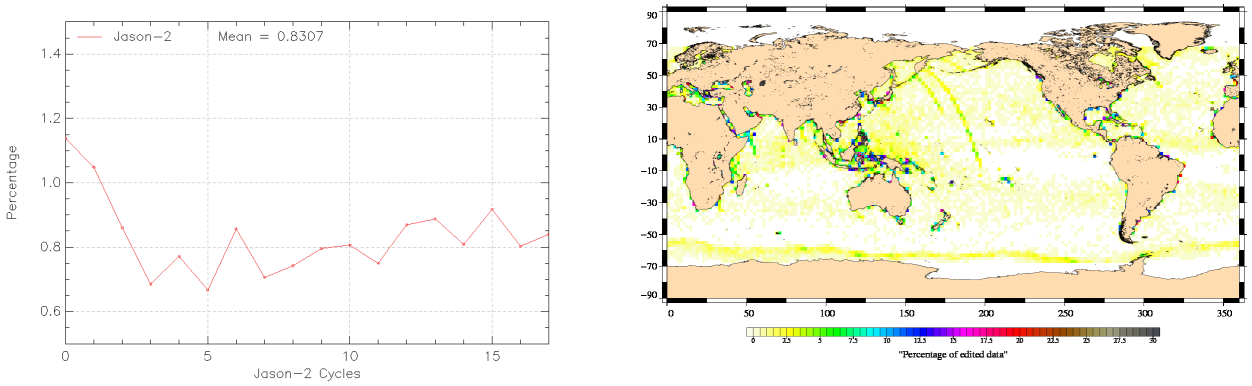

Figure 15: *Percentage of edited measurements by square off-nadir angle criterion. Left: Cycle per cycle monitoring. Right: Map over a sixth month period (cycles 0 to 17).*

3.2.14. Sea state bias correction

The percentage of edited measurements due to sea state bias correction criterion is represented in figure 16. The percentage of edited measurements is about 0.18% and shows no drift.
The map 16 shows that edited measurements are mostly found in equatorial regions near coasts.

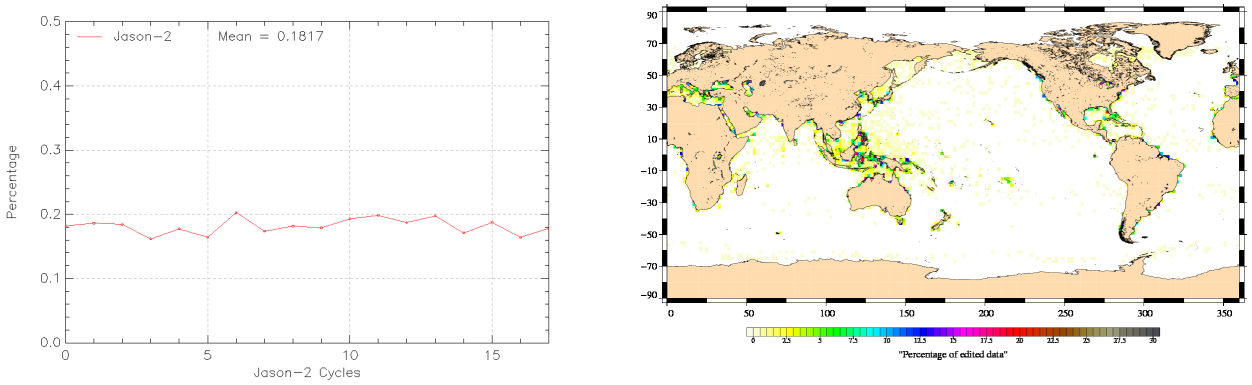

Figure 16: *Cycle per cycle percentage of edited measurements by sea state bias criterion (left). Right: Map of percentage of edited measurements by sea state bias criterion over a sixth month period (cycles 0 to 17).*

3.2.15. Altimeter wind speed

The percentage of edited measurements due to altimeter wind speed criterion is represented in figure 17. It is about 0.65% and shows a small decrease, which might be part of an annual signal. The measurements are edited, because they have default values. This is the case when sigma0 itself is at default value, or when it shows very high values (higher than 25 dB), which occur during sigma bloom and also over sea ice. Indeed, the wind speed algorithm (which uses backscattering coefficient and significant wave height) can not retrieve values for sigma0 ¿ 25 dB.
The map 17 showing percentage of measurements edited by altimeter wind speed criterion is correlated with maps 16 and 10.

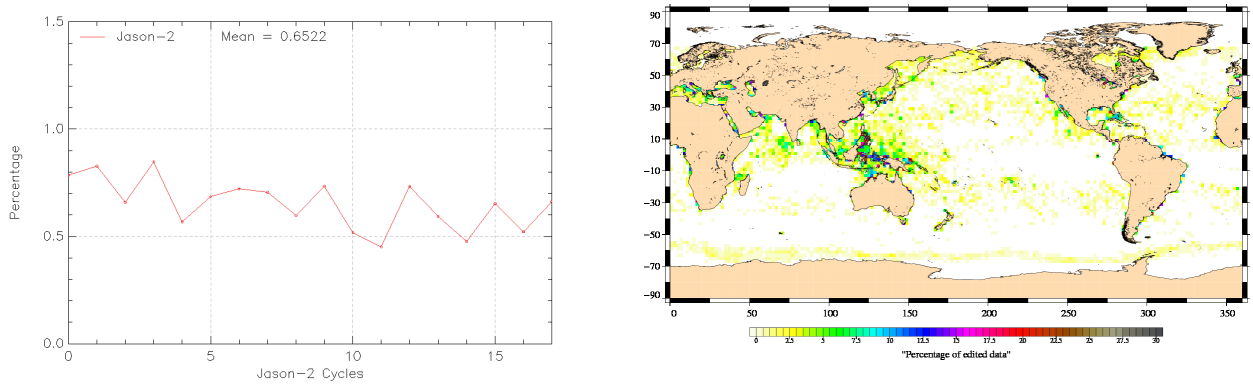

Figure 17: *Percentage of edited measurements by altimeter wind speed criterion. Left: Cycle per cycle monitoring. Right: Map over a sixth month period (cycles 0 to 17).*

3.2.16. Ocean tide correction

The percentage of edited measurements due to ocean tide correction criterion is represented in figure 18. It is about 0.07% and shows probably a beginning of an annual signal. The ocean tide correction is a model output, there should therefore be no edited measurements. Indeed there are no measurements edited in open ocean areas, but only very few near coasts or in lakes or rivers (see map 18). These measurements are mostly at default values.
Some of these lakes are in high latitudes and therefore periodically covered by ice. This explains the annual signal visible in figure 18.

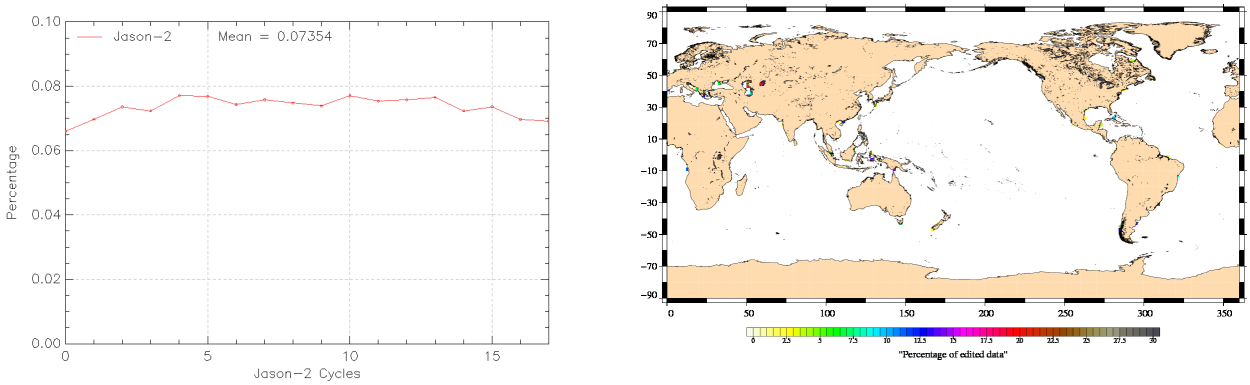

Figure 18: *Percentage of edited measurements by ocean tide criterion. Left: Cycle per cycle monitoring. Right: Map over a sixth month period (cycles 0 to 17).*

3.2.17. Sea surface height

The percentage of edited measurements due to sea surface height criterion is represented in figure 19. It is about 0.28% and shows no drift. The measurements edited by sea surface height criterion are mostly found near coasts in equatorial regions (see map 19)

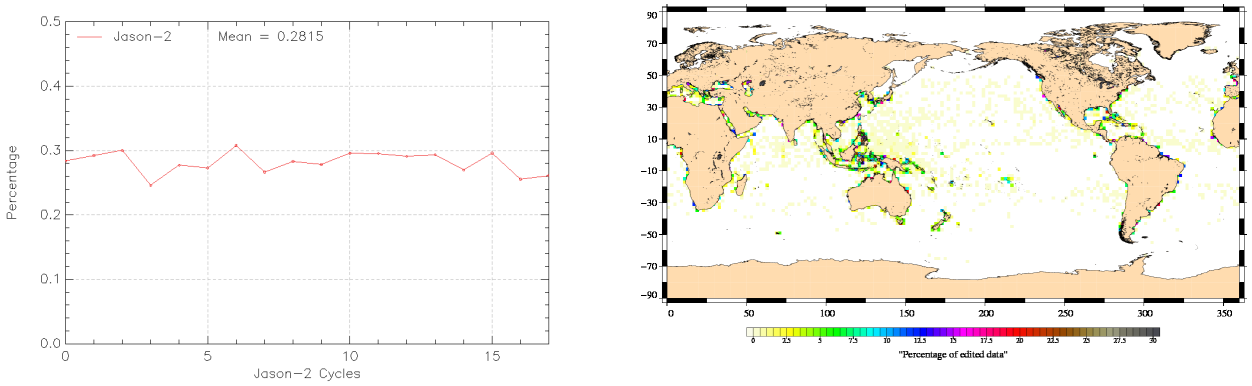

Figure 19: *Percentage of edited measurements by sea surface height criterion. Left: Cycle per cycle monitoring. Right: Map over a sixth month period (cycles 0 to 17).*

3.2.18. Sea level anomaly

The percentage of edited measurements due to sea level anomaly criterion is represented in figure 20. It is about 0.69% and shows no drift. The graph is quite similar to the one in figure 13 (showing the percentage of measurements edited by AMR), as the SLA clip contains, among other parameters, the radiometer wet troposphere correction.
Whereas the map in figure 20 allows us to plot the measurements edited due to sea level anomaly out of thresholds (after applying all other threshold criteria). There are only very few measurements, principally located in Caspian Sea.

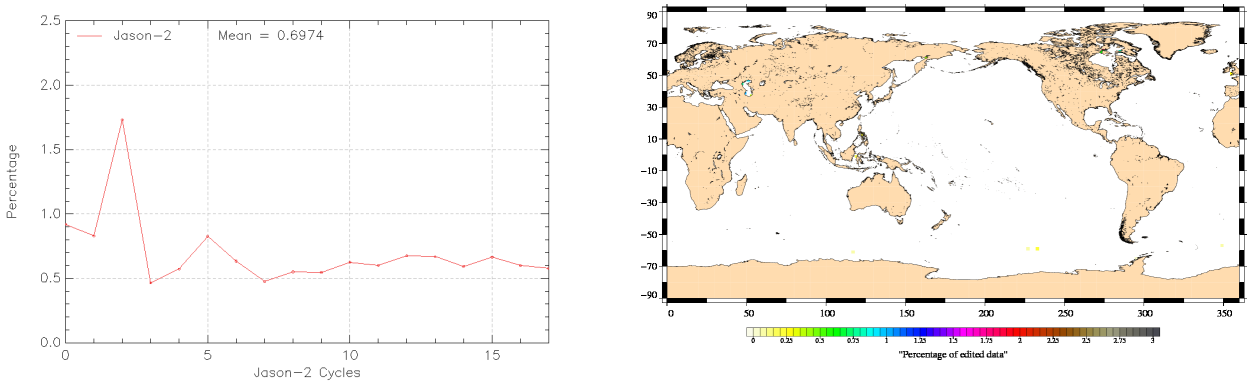

Figure 20: *Percentage of edited measurements by sea level anomaly criterion. Left: Cycle per cycle monitoring. Right: Map over a sixth month period (cycles 0 to 17).*

4. Monitoring of altimeter and radiometer parameters

4.1. Methodology

Both mean and standard deviation of the main parameters of Jason-2 have been monitored since the beginning of the mission. Moreover, a comparison with Jason-1 parameters has been performed: it allows us to monitor the bias between the parameters of the 2 missions.

Till Jason-2 cycle 20, Jason-2 and Jason-1 ground tracks are on the same ground track and are spaced out about 1 minute apart. The mean of the Jason-1 - Jason-2 differences can be computed using a point by point repeat track analysis.

4.2. 20 Hz Measurements

The monitoring of the number and standard deviation of 20 Hz elementary range measurements used to derive 1 Hz data is presented here. These two parameters are computed during the altimeter ground processing. For Jason-1, before performing a regression to derive the 1 Hz range from 20 Hz data, a MQE (mean quadratic error) criterion is used to select valid 20 Hz measurements. This first step of selection consists in verifying that the 20 Hz waveforms can be approximated by a Brown echo model (Brown, 1977 [1]) (Thibaut et al. 2002 [9]). Then, through an iterative regression process, elementary ranges too far from the regression line are discarded until convergence is reached. Thus, monitoring the number of 20 Hz range measurements and the standard deviation computed among them is likely to reveal changes at instrumental level.
The Jason-1 MQE threshold are not applicable to Jason-2, using those thresholds would edit more measurements than necessary. Therefore the Jason-2 MQE threshold has been set to default, leading to no editing based on MQE values.

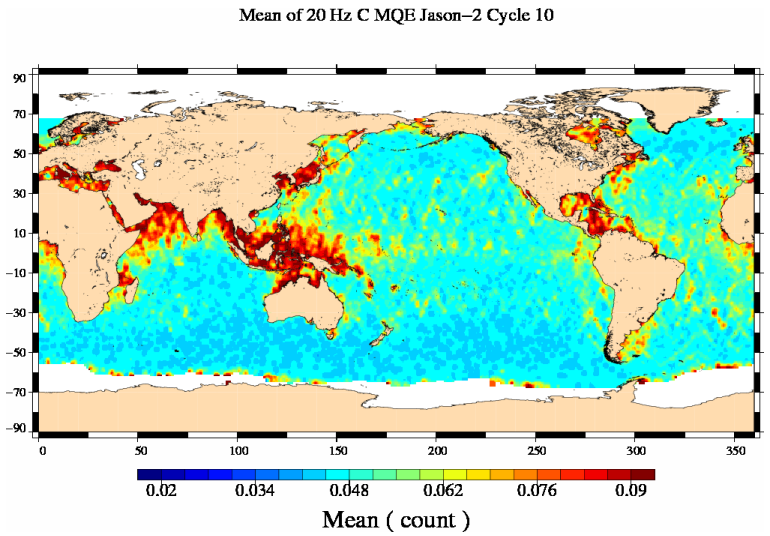

Figure 21: *Map of 20 Hz C-band MQE for Jason-2 cycle 10.*

4.2.1. 20 Hz measurements number in Ku-Band and C-Band

Figures 22 and 23 show on the left the daily monitoring of the mean and standard deviation of Jason-1 - Jason-2 differences of 20-Hz measurements number in Ku-Band and C-band. Besides a slight increase in mean and decrease in standard deviation is visible, probably related to an annual cycle. They are quite stable and do not show any anomaly. Number of 20 Hz range measurements is slightly higher for Jason-2 than for Jason-1, since mean of Jason-1 - Jason-2 difference is slightly negatif (-0.1 for Ku-band and -0.2 for C-band). The regions where Jason-1 has less elementary range measurements are especially located around Indonesia, as shown on map of Jason-1 - Jason-2 differences (right side of figures 22 and 23). They seem to be correlated to high MQE values (see figure 21), especially in C-band. Since the current MQE criterium for Jason-2 does not eliminate 20 Hz measurements used for 1 Hz compression (whereas for Jason-1 this is the case), number of 20 Hz range measurements is smaller for Jason-1 than for Jason-2 in high MQE areas.

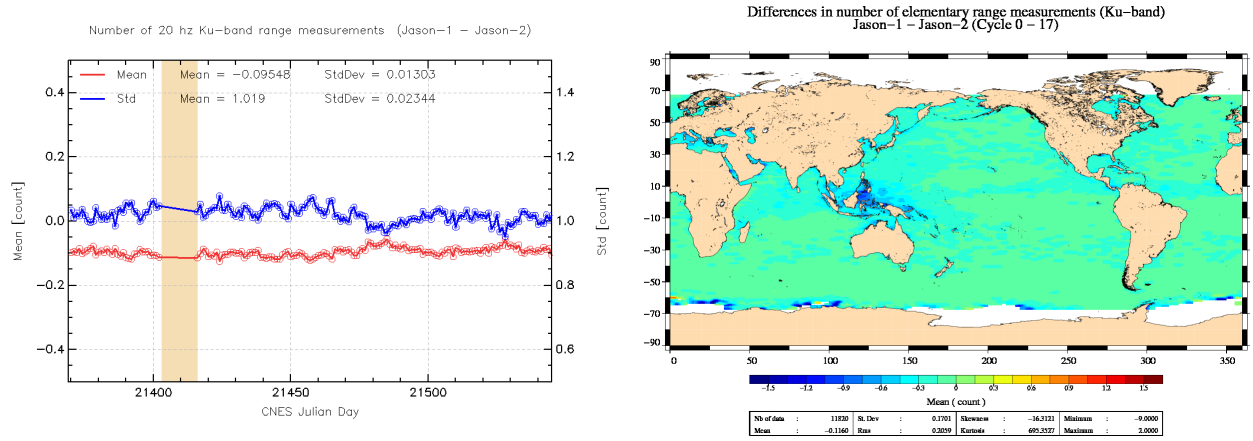

Figure 22: *Daily monitoring of mean and standard deviation of Jason-1 - Jason-2 differences for number of elementary 20 Hz Ku-band range measurements (left) and map showing mean of Jason-1 - Jason-2 differences over cycles 0 to 17 (right).*

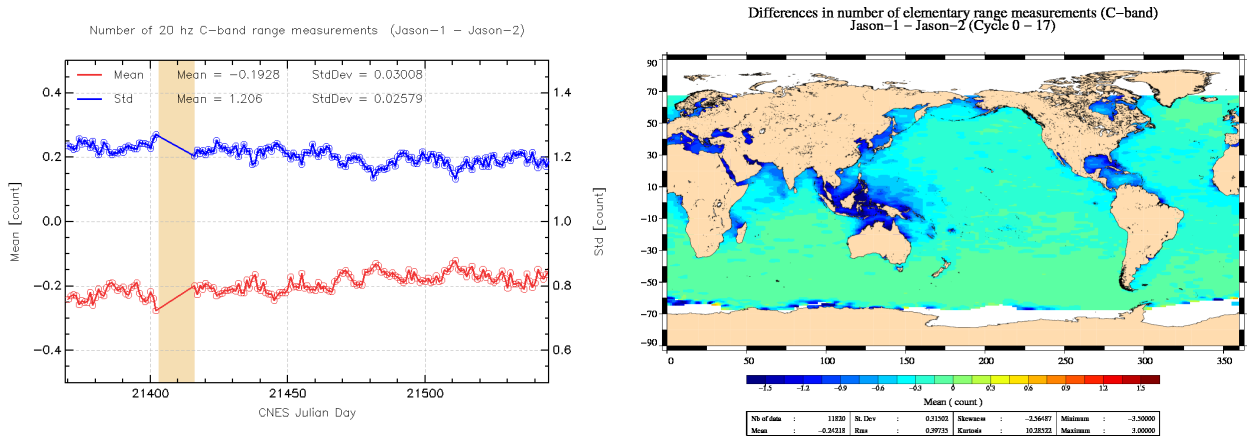

Figure 23: *Daily monitoring of mean and standard deviation of Jason-1 - Jason-2 differences for number of elementary 20 Hz C-band range measurements (left) and map showing mean of Jason-1 - Jason-2 differences over cycles 0 to 17 (right).*

4.2.2. 20 Hz measurements standard deviation in Ku-Band and C-Band

Figure 24 and 25 show daily monitoring of Jason-1 - Jason-2 difference of standard deviation of the 20 Hz measurements in Ku-Band and C-Band (on the left). No trend neither anomaly has been detected. C-Band standard deviation of the 20 Hz measurements rms is noisier than those of Ku-Band. This is directly linked to the C-band standard deviation which is higher than the Ku, as the onboard averaging is performed over less waveforms leading to an increased noise.

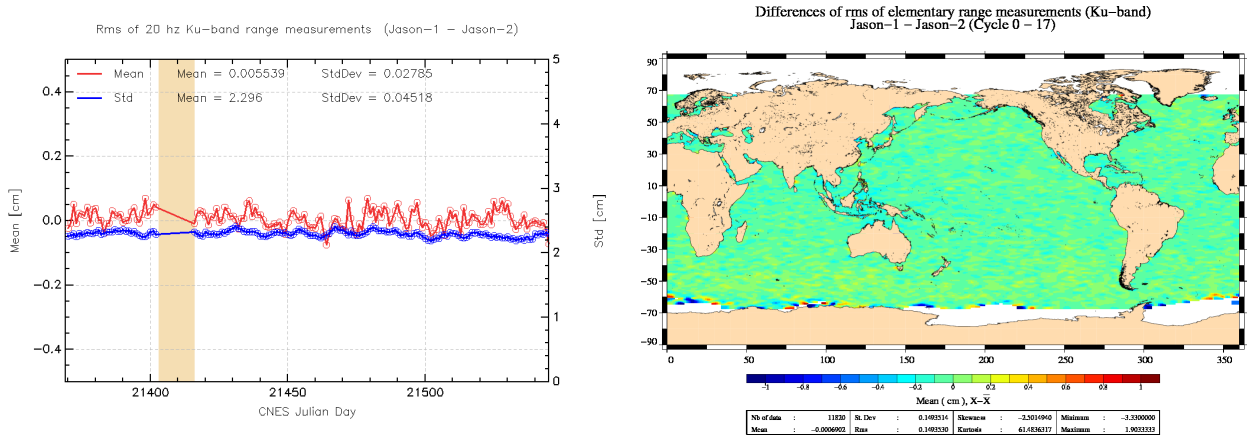

Figure 24: *Daily monitoring of mean and standard deviation of Jason-1 - Jason-2 differences for the rms of elementary 20 Hz Ku-band range measurements (left) and map showing mean of Jason-1 - Jason-2 differences over cycles 0 to 17 (right).*

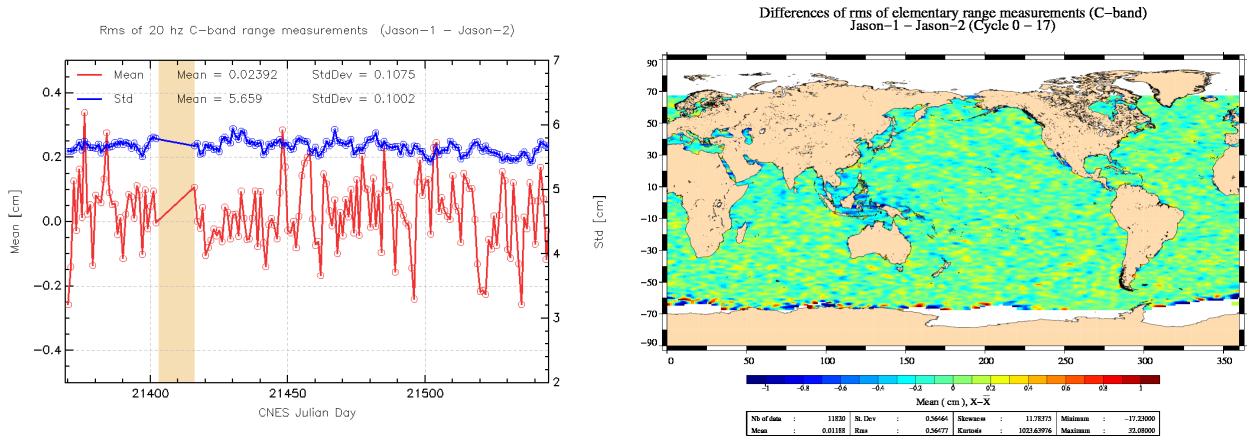

Figure 25: *Daily monitoring of mean and standard deviation of Jason-1 - Jason-2 differences for rms of elementary 20 Hz C-band range measurements (left) and map showing mean of Jason-1 - Jason-2 differences over cycles 0 to 17 (right).*

4.3. Off-Nadir Angle from waveforms

The off-nadir angle is estimated from the waveform shape during the altimeter processing. The square of the off-nadir angle, averaged on a daily basis, has been plotted for Jason-1 and Jason-2 on the left side of figure 26, whereas the right side shows the histograms over one cycle. The mean values are slightly positive. This mean value is not significant in terms of actual platform mispointing. Mispointing of Jason-2 is quite stable, close to 0.01 deg2 (probably related to small differences in antenna aperture values used for Jason-1 and Jason-2 processing). Whereas Jason-1 may show higher values (related to the reduced tracking performance of both star trackers, especially during fixed-yaw).

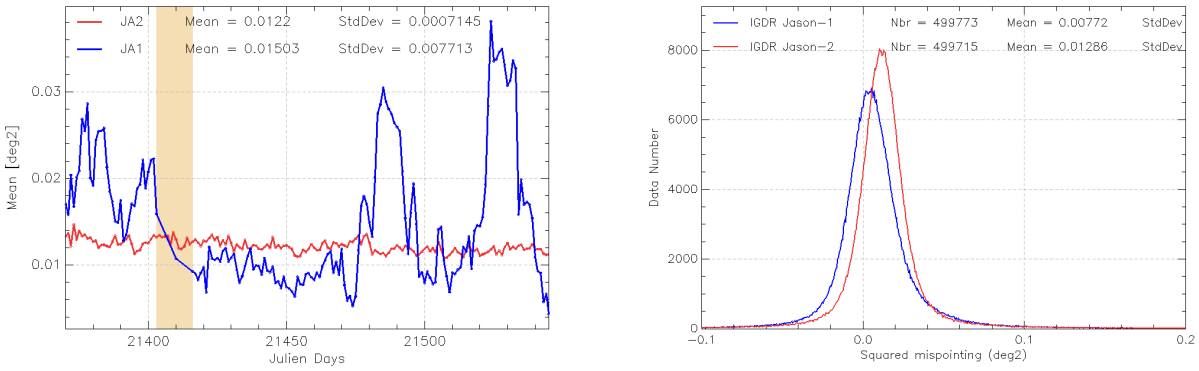

Figure 26: *Square of the off-nadir angle deduced from waveforms (deg^2) for Jason-1 and Jason-2: Daily monitoring (left), histograms for Jason-2 cycle 10 (Jason-1 cycle 249).*

4.4. Significant wave height

4.4.1. Ku-band SWH

The Ku-band significant wave height (SWH) shows a very good agreement between Jason-2 and Jason-1 (figure 27). Daily monitoring of mean of the differences shows no drift. Global SWH mean difference is -1 cm. Higher values are located near Indonesia or Mediterranean Sea, but otherwise it is quite homogeneous.

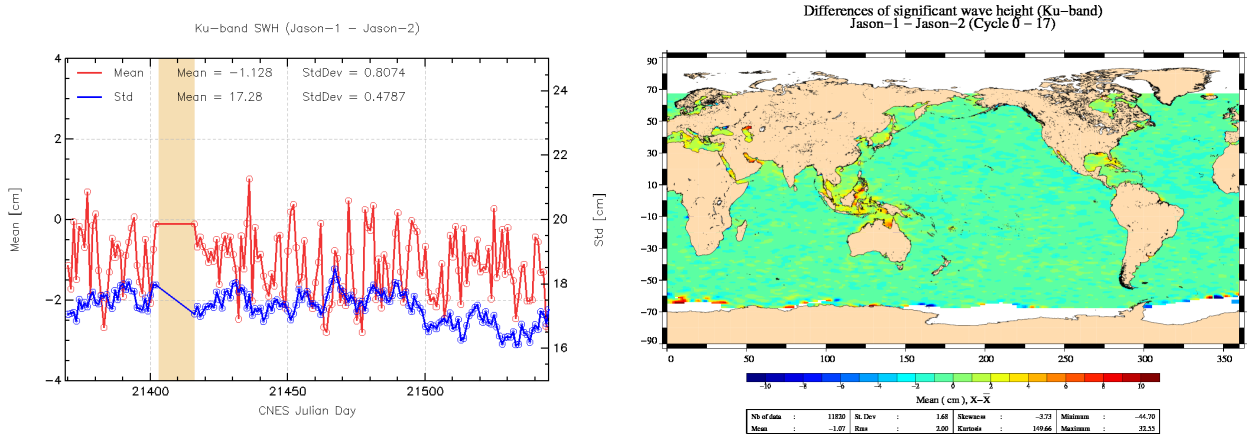

Figure 27: *Daily monitoring of mean and standard deviation of Jason-1 - Jason-2 differences for Ku-band SWH (left) and map showing mean of Jason-1 - Jason-2 differences over cycles 0 to 17 (right).*

4.4.2. C-band SWH

Figure 28 shows global statistics of Jason-1 - Jason-2 difference of C-band SWH. The daily mean difference shows a slight decrease (figure 28 left). The mean difference is -6 mm, but regional differences may reach 10 cm, especially around Indonesia or in the Mediterranean Sea. This is strongly correlated to regions with high MQE values (figure 21 and section 7.2.).

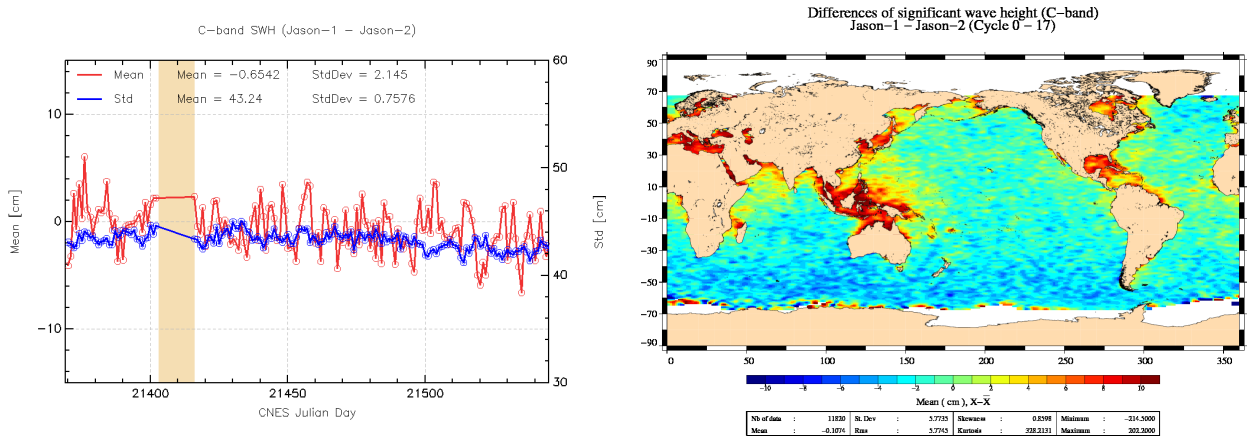

Figure 28: *Daily monitoring of mean and standard deviation of Jason-1 - Jason-2 differences for C-band SWH (left) and map showing mean of Jason-1 - Jason-2 differences over cycles 0 to 17 (right).*

4.5. Backscatter coefficient

4.5.1. Ku-band Sigma0

The Jason-2 Ku-band backscattering coefficient shows good agreement with Jason-1 as visible in map of mean differences (right side of figure 29) and in daily monitoring (left side of figure 29). The global bias with JA1 is weak (0.1 dB in Ku-band). In comparison, the global bias between Jason-1 and Topex/Poseidon was about 2.4 dB. Nevertheless a small signal (0.1 dB) in Ku-band differences is detected in daily monitoring (figure 29). This seems correlated to Jason-1 mispointing.

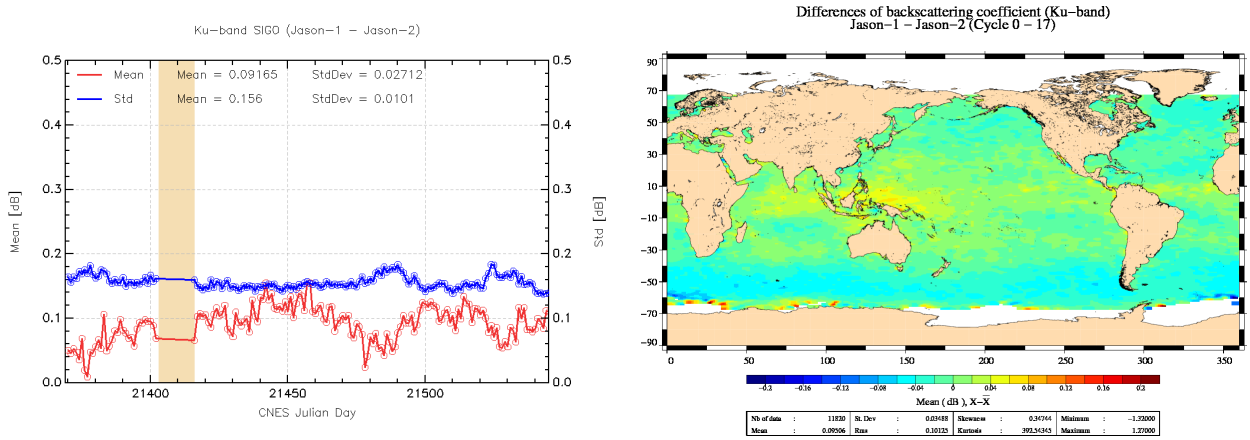

Figure 29: *Daily monitoring of mean and standard deviation of Jason-1 - Jason-2 differences for Ku-band Sigma0 (left) and map showing mean of Jason-1 - Jason-2 differences over cycles 0 to 17 (right).*

4.5.2. C-band Sigma0

The Jason-2 C-band backscattering coefficient shows also good agreement with Jason-1 as plotted in map of mean differences (right side of figure 30) and in daily monitoring (left side of figure 30). The global bias with JA1 is weak (0.2 dB in C-band). It was slightly higher during the first 6 cycles.

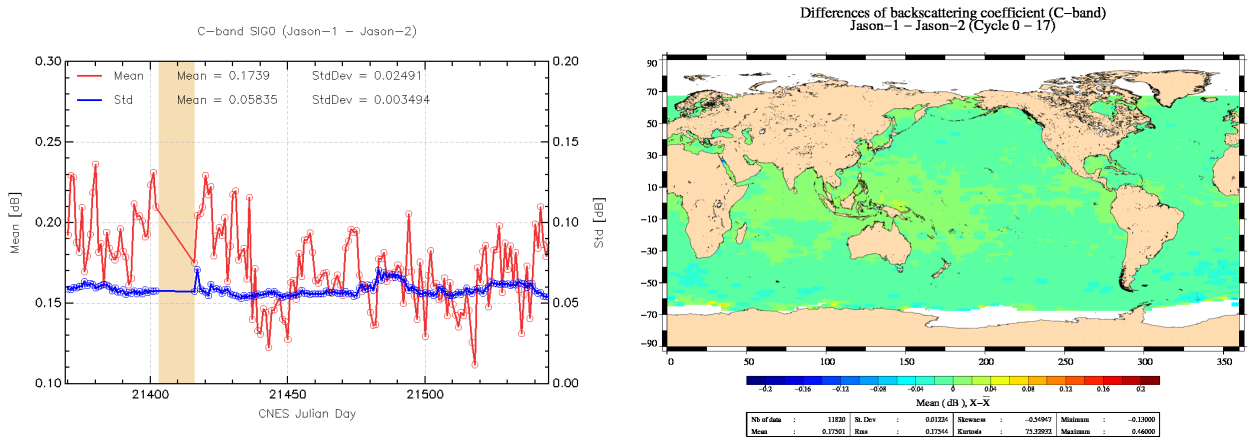

Figure 30: *Daily monitoring of mean and standard deviation of Jason-1 - Jason-2 differences for C-band Sigma0 (left) and map showing mean of Jason-1 - Jason-2 differences over cycles 0 to 17 (right).*

4.6. Dual-frequency ionosphere correction

The dual frequency ionosphere corrections derived from the Jason-2 and Jason-1 altimeters show a mean difference of -0.9cm (figure 31 (left)), linked to the Ku- and C-Band relative bias. This difference is quite stable, with daily variations lower than 2 mm. The map of local differences (figure 31 right) shows increased differences near Indonesia (probably correlated to high MQE values).

Notice that, as for TOPEX and Jason-1 (Le Traon et al. 1994 [6]), it is recommended to filter the Jason-2 dual frequency ionosphere correction before using it as a SSH geophysical correction (Chambers et al. 2002 [3]). A low-pass filter has thus been used to remove the noise of the correction in all SSH results presented in the following sections.

Plotting difference of non-filtered ionospheric correction between Jason-2 and Jason-1 versus Jason-1 ionospheric correction shows an apparent scale error, which disappears when using filtered data (see figure 32). As currently ionosphere correction is very low, the ionosphere noise is of the same order of magnitude as the ionosphere correction itself. Therefore plotting the difference of non-filtered dual-frequency ionospheric correction versus dual-frequency ionospheric correction induces an apparent scale error.

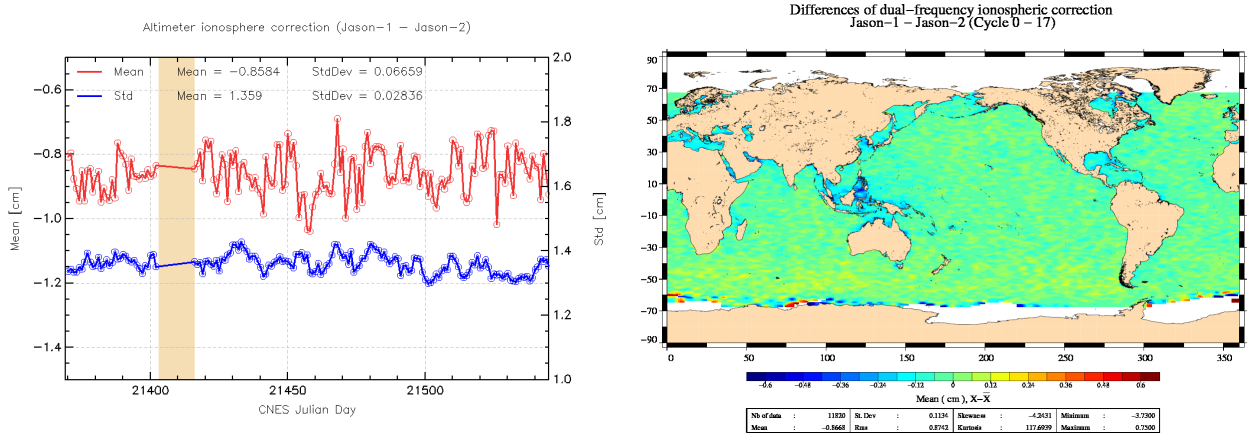

Figure 31: *Daily monitoring of mean and standard deviation of Jason-1 - Jason-2 differences for dual-frequency ionospheric correction (left) and map showing mean of Jason-1 - Jason-2 differences over cycles 0 to 17 (right).*

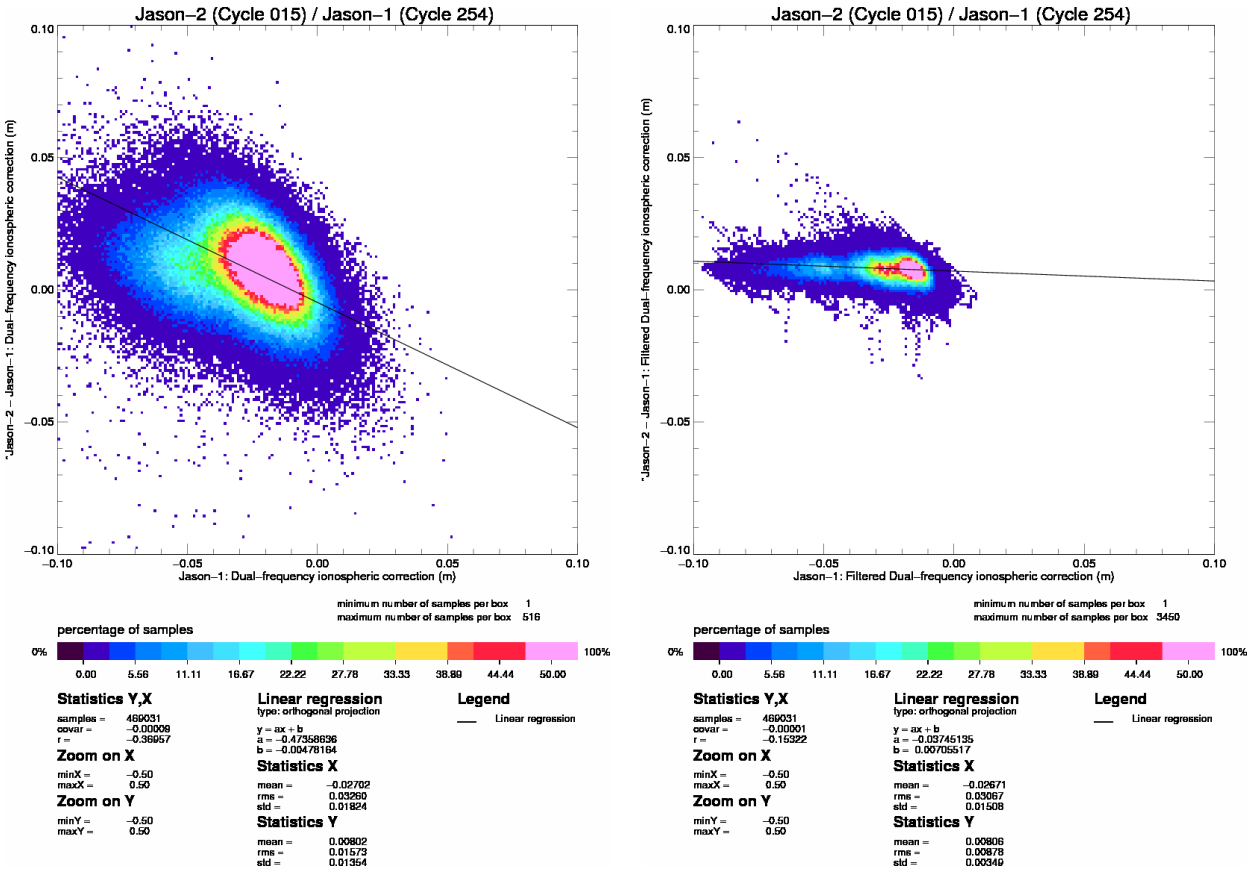

Figure 32: *Diagram of dispersion of Jason-2 - Jason-1 versus Jason-1 dual-frequency ionosphere correction for Jason-2 cycle 15. Left: non-filtered, right: filtered.*

4.7. AMR Wet troposphere correction

Figure 33 shows on the left side the daily monitoring of the difference of radiometer wet troposphere correction between the two missions (JMR - AMR) on the IGDR products. AMR is globally wetter than JMR (0.4 cm), especially near equator and coasts (right side of figure 33). Several features can be observed in the daily monitoring:

- a small decrease of about 1 mm during the first 8 days (cycle 0). This might be related to the heating of the AMR.
- between cycle 1 and cycle 3, difference between the two radiometers is quite stable.
- after the Jason-1 safehold mode which occured in the middle of Jason-2 cycle 3 till end of Jason-2 cycle 4, difference between JMR and AMR shows several large anomalies reaching up to 7 mm. This is due to odd behaviour of JMR, as described in the next section.
- for the last cycles difference between JMR and AMR is increasing.

For the data shown here (IGDR products for cycles 0 to 17), the same AMR characterization file was in use. It only evolved in February 2009.

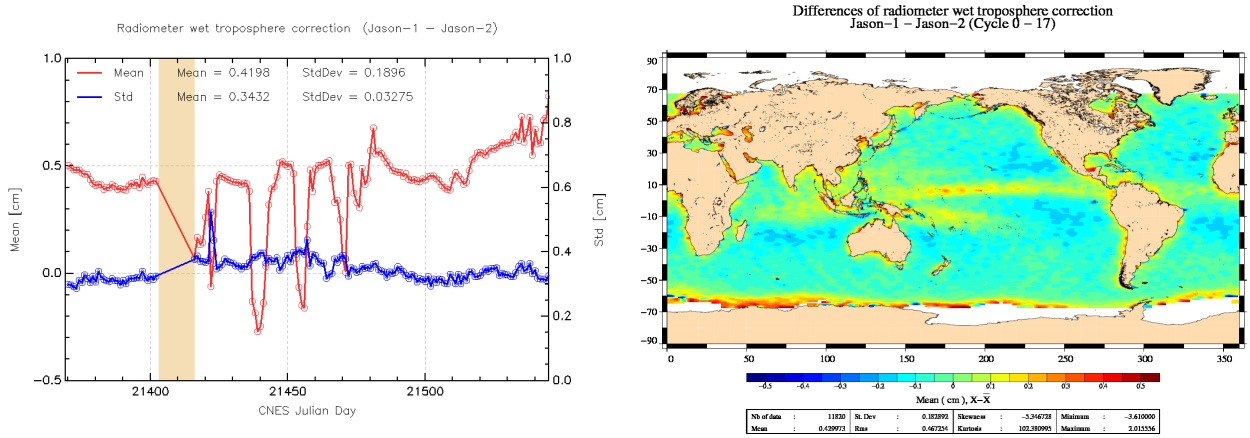

Figure 33: *Daily monitoring of mean and standard deviation (left) of Jason-1 - Jason-2 radiometer wet troposphere correction. Map showing mean of Jason-1 - Jason-2 differences over cycles 0 to 17 (right).*

Daily monitoring of JMR - AMR 34 GHz brightness temperature shows jumps which coincide sometimes, but not always with Jason-2 yaw maneuvers (see figure 34). These jumps seem to be originated in AMR. They will likely be accounted for in GDR products thanks to the cyclic radiometer characterization file update provided by the ARCS system ([2].)

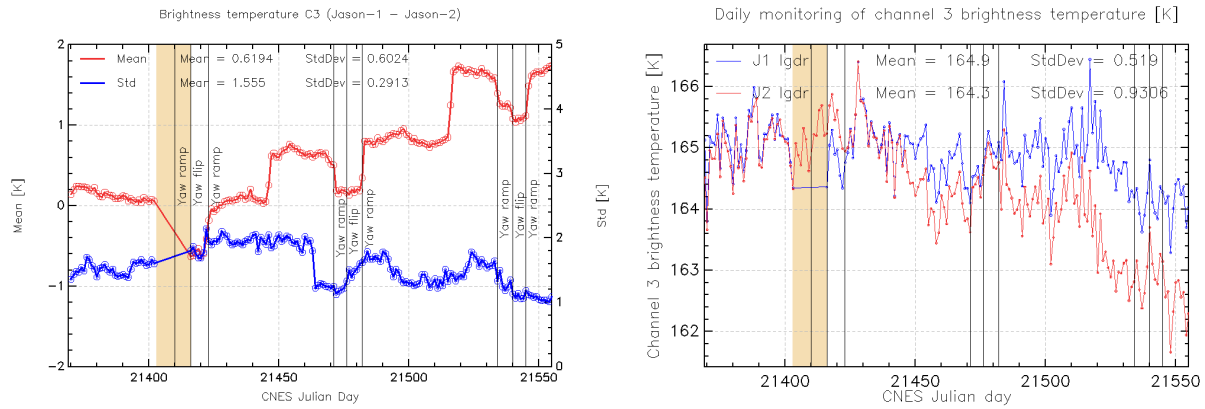

Figure 34: *Monitoring of daily mean and standard deviation of Jason-1 - Jason-2 34 GHz brightness temperature (left). Daily moinitoring of 34 HGz brightness temperature of Jason-1 and Jason-2. Black lines indicate yaw maneuvers.*

4.7.1. Comparison with the ECMWF model

Wet troposphere correction from radiometers may experience drifts or jumps. Model wet troposphere correction may also be not stable in time as it undergoes model evolutions. Therefore comparing different radiometer wet troposphere corrections with ECMWF model is important.
Figure 35 shows daily monitoring of difference of radiometer - model wet troposphere correction for Jason-2, Jason-1 and Envisat. An odd behaviour between Jason-2 cycles 5 and 11 (Julian day 21415 to 21485) is noticed for Jason-1. Figure 35 shows indeed, that radiometer minus model wet troposphere corrections decreases slightly for Jason-2, whereas it shows large fluctuations for Jason-1. This is probably related to the safehold mode which occured during Jason-1 cycle 242 and 243.
Over the period of Julian day 21415 to approximatively Julian day 21515, radiometer - model difference shows a decreasing trend for Jason-1, as well as for Jason-2. This is also the case for Envisat radiometer - model difference. For this period Jason-2 and Envisat satellite show a good agreement. Nevertheless since Julian day 21515 (beginning of Jason-2 cycle 15), radiometer - model difference continues to decrease for Jason-2, whereas it slightly increases for Jason-1 and Envisat.

AMR antenna is wider than JMR one's, which allows to improve the radiometer correction close to the coasts. This is visible on figure 36, showing differences between radiometer and model wet troposphere correction in function of coast distance for Jason-2 cycle 10. Far away from coasts, behaviour of JMR and AMR is similar.

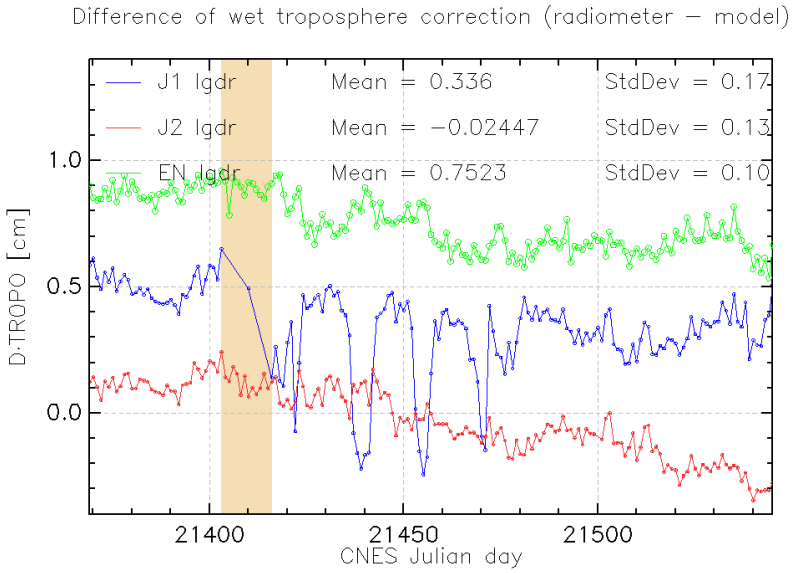

Figure 35: *Daily monitoring of radiometer and ECMWF model wet troposphere correction differences for Jason-1 (blue), Jason-2 (red) and Envisat (green).*

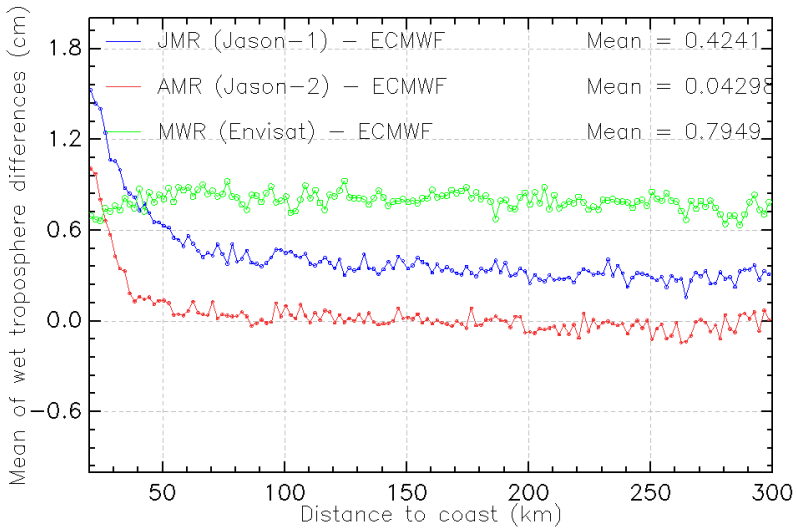

Figure 36: *Comparison of differences between radiometer and ECMWF model wet troposphere correction in function of coast distance for several altimeter missions: Jason-2 (red), Jason-1 (blue), Envisat (green).*

5. SSH crossover analysis

5.1. Overview

Crossover differences are systematically analyzed to estimate data quality and the Sea Surface Height (SSH) performances. They are compared to Jason-1 crossover performances. Impact of different type of orbits (Doris navigator (from Ogdr), MOE (from Igdr), and POE (from Gdr)) are shown. SSH crossover differences are computed on a one cycle basis, with a maximum time lag of 10 days, in order to limit the effects of ocean variability which are a source of error in the performance estimation. The main SSH calculation for Jason-2 and Jason-1 are defined below.

$$SSH = Orbit - Altimeter\ Range - \sum_{i=1}^{n} Correction_i$$

with $Jason-1/Jason-2\ Orbit = MOE\ CNES\ orbit$ for IGDR products, or $POE\ CNES\ orbit$ for GDR products, or $DIODE\ orbit$ for OGDR products, and

$$\begin{aligned}\sum_{i=1}^{n} Correction_i &= Dry\ troposphere\ correction : new\ S1\ and S2\ atmospheric\ tides\ applied \\ &+ Combined\ atmospheric\ correction :\ high\ resolution\ MOG2D\ and\ inverse\ barometer \\ &+ Radiometer\ wet\ troposphere\ correction \\ &+ Filtered\ dual\ frequency\ ionospheric\ correction \\ &+ Non\ parametric\ sea\ state\ bias\ correction \\ &+ Geocentric\ ocean\ tide\ height,\ GOT\ 2000 :\ S1\ atmospheric\ tide\ is\ applied \\ &+ Solid\ earth\ tide\ height \\ &+ Geocentric\ pole\ tide\ height\end{aligned}$$

5.2. Mean of SSH crossover differences

The mean of SSH crossover differences represents the average of SSH differences between ascending and descending passes. This diagnostic allows us to estimate the SSH homogeneity between ascending and descending passes. Differences of SSH between ascending and descending should be close to zero.

5.2.1. Maps after averaging per boxes

The map build by averaging per box the mean of SSH crossover differences over the whole period of available IGDR (cycle 0 to 17) has been plotted in figure 37 for Jason-2 (on left) and Jason-1 (on right). The Jason-2 map is very homogeneous whereas large features between ± 5 cm are highlighted on the Jason-1 map.
To complete this analysis, the same maps have been computed after replacing the MOE by the POE orbit in the SSH calculation for both satellites over a period slightly shorter (cycle 1 to 14) as plotted in figure 38. Both maps are now very similar and very homogeneous. Especially, the

Jason-1 map does not display the large patches observed using the MOE orbit. This indicates that the Jason-2 MOE performances are better than the Jason-1 ones which is probably impacted by some problems under investigation by the CNES POD team.

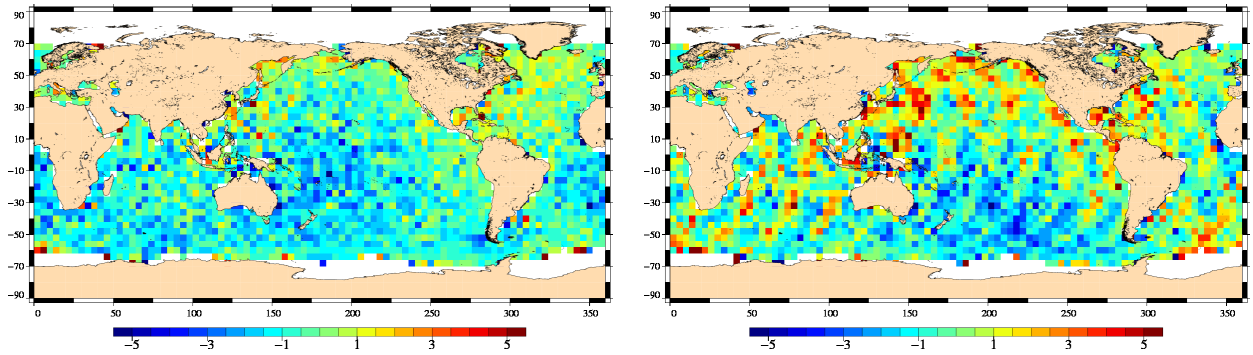

Figure 37: *Map of mean of SSH crossovers differences for Jason-2 cycle 0 to 17 (left) and Jason-1 over the same period (right) using MOE*

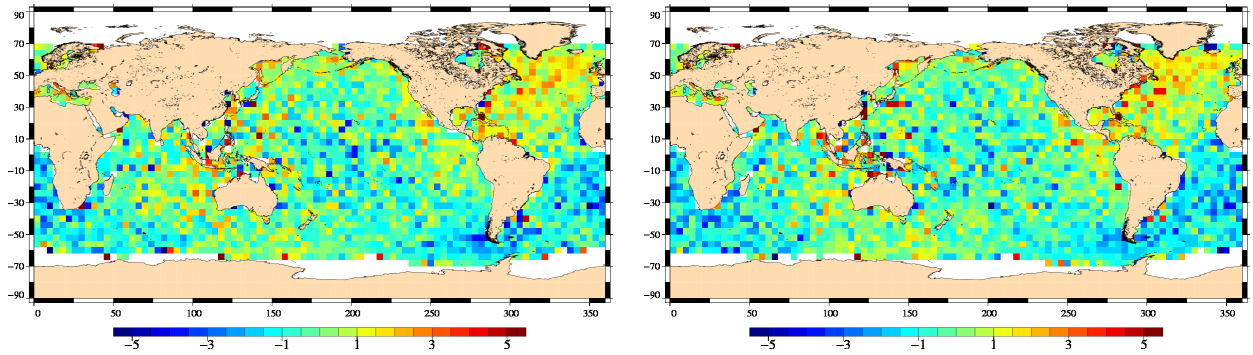

Figure 38: *Map of mean of SSH crossover differences for Jason-2 cycle 1 to 14 (left) and Jason-1 over the same period (right) using POE*

5.2.2. Cycle by cycle monitoring

The monitoring of the mean of SSH crossover differences since the beginning of the period shows the good stability of Jason-2 SSH at crossovers as plotted in figure 39 on the left. Using MOE orbit, Jason-2 SSH curve is more stable than Jason-1 one's, in agreement with previous results (figure 37 on right). In the same chart, both Jason-1 and Jason-2 curves derived from POE orbits have been plotted. They have a very similar behavior: very stable and close to 0.
The same curves using DIODE orbit from OGDR products for both satellite are plotted in figure 39 on the right. Of course, they are significantly less stable than using MOE or POE orbits. But Jason-2 curve is better centered than Jason-1 one. The Jason-2 DIODE orbit calculation has been largely improved.

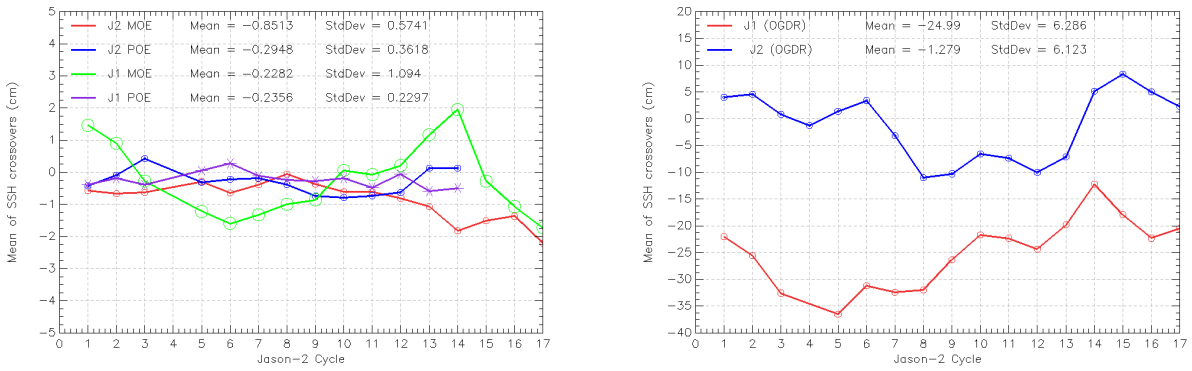

Figure 39: *Monitoring of mean of SSH crossover differences for Jason-2 and Jason-1 using MOE and POE orbits*

5.3. Standard deviation of SSH crossover differences

5.3.1. Maps after averaging per boxes

Maps build by averaging per box the standard deviation of SSH crossover differences have been plotted using MOE orbit (figure 40) and POE orbit (figure 41) for Jason-2 (on the left) and Jason-1 (on the right). These maps have been computed over all the Jason-2 period. They do not bring out anomalies. The usual high variability areas are highlighted.

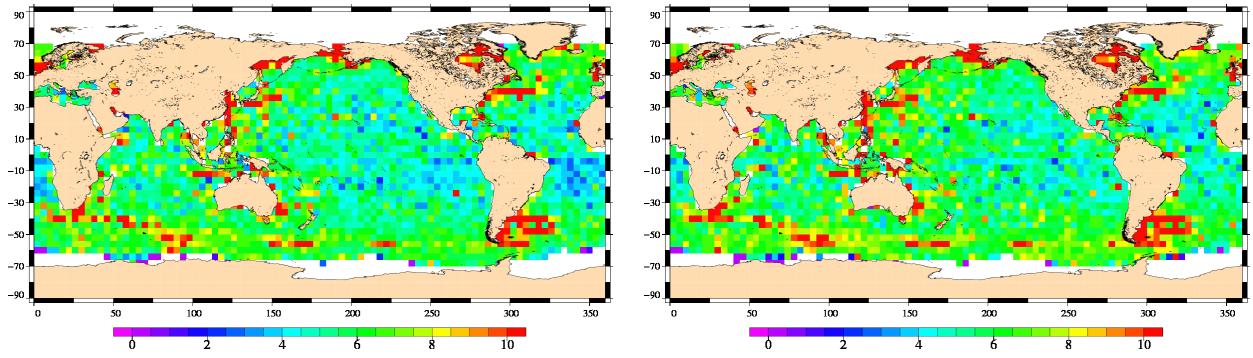

Figure 40: *Map of standard deviation of SSH crossover differences for Jason-2 cycle 0 to 17(left) and Jason-1 over the same period (right) using MOE orbit*

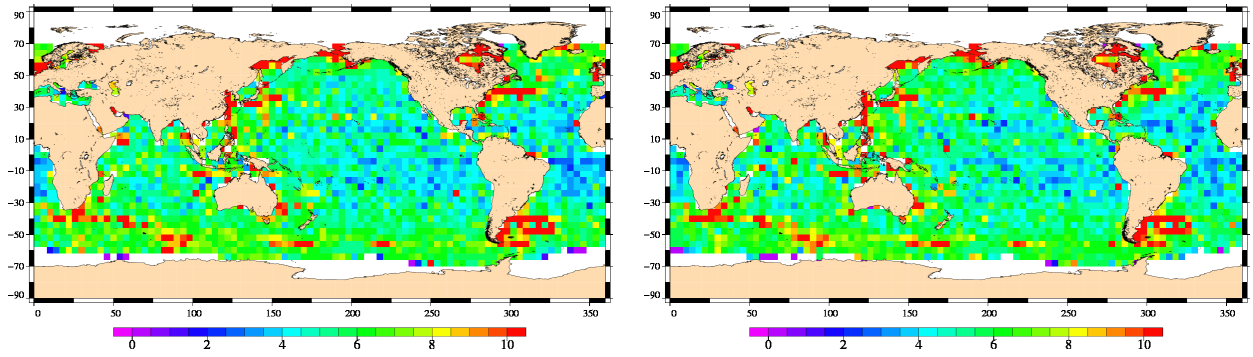

Figure 41: *Map of standard deviation of SSH crossover differences for Jason-2 cycle 1 to 14 (left) and Jason-1 over the same period (right) using POE orbit*

5.3.2. Cycle by cycle monitoring

The cycle per cycle standard deviation of SSH crossover differences allows us to follow the performance of the altimeter system. In order to provide reliable estimates, the variable effects due to the physical processes have to be removed. The following crossover selections are thus applied: areas with shallow waters (bathymetry $> -1000m$), high ocean variability (> 20 cm) and high latitudes ($> |50|$ degrees) have been removed.
The associated statistics are plotted in figure 42 using the POE and MOE orbits on the left chart and the DIODE orbit from OGDR on the right chart. Concerning the curves with the MOE orbit,

the Jason-2 performances are very good and better than Jason-1 ones. As previously and already mentioned, the reduction of Jason-1 SSH performances is in relationship with the MOE orbit calculation impacted by some problems under investigations. Using POE orbit for both satellites, the SSH performances are similar and very good: close to 5 cm rms in average. Replacing the precise orbits by the DIODE orbit in the SSH calculation increases significantly the statistics as expected. This is especially true for Jason-1, since the SSH performances are close to 14 cm rms in average which is prohibitive for oceanic applications. On the other hand, Jason-2 SSH performances are between 7 and 8 cm rms from cycle 9 onwards. Before this cycle, SSH performances were reduced because the DIODE software on-board was no completely well tuned. This good level of performances with a real-time orbit is a main improvement in altimeter data allowing us to intend the use of Jason-2 OGDR products in operational systems such as DUACS.

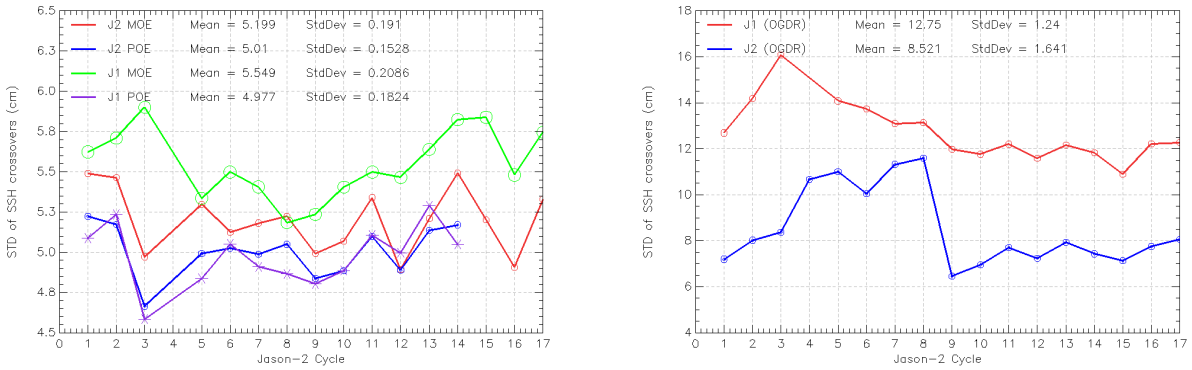

Figure 42: *Cycle per cycle monitoring showing mean (left) and standard deviation (right) of SSH crossovers for Jason-2 and Jason-1 using MOE and real time orbit.*

5.4. Estimation of pseudo time-tag bias

The pseudo time-tag bias (α) is calculated performing a linear regression from SSH crossovers and the altimeter radial speed ($\dot{H}$):

$$\Delta SSH = \alpha \dot{H}$$

The pseudo time-tag bias is estimated cycle by cycle and monitored from the beginning of an altimeter mission in order to determine a potential bias in the precise data datation. This kind of diagnostic allowed us to detect for Jason-1 a time-tag bias close to 0.28 ms after removing a strong 60-day signal. The impact on the Jason-1 SSH is weak but not negligible close to $\pm$ 0.5 cm (it is opposite for ascending and descending passes). An additional correction has been taken into account in Jason-1 GDR-C product to correct this error. To date, the origin of this error is misunderstood. It might be due to a true datation error in the measurements, but also a datation error in orbit calculation or other unknown errors in the altimeter system assimilated as a pseudo error of datation trough our empirical method.
It is thus very interesting to monitor this pseudo time-tag bias for Jason-2 in comparison with Jason-1 as plotted in the following figure 43. After 18 cycles, the estimates are very similar for both satellites with a 60 day-signal and average bias between -0.25 and -0.3 ms. Finally the potential datation error observed on Jason-1 data as previously mentioned is similar for Jason-2. This error should be thoroughly investigated.

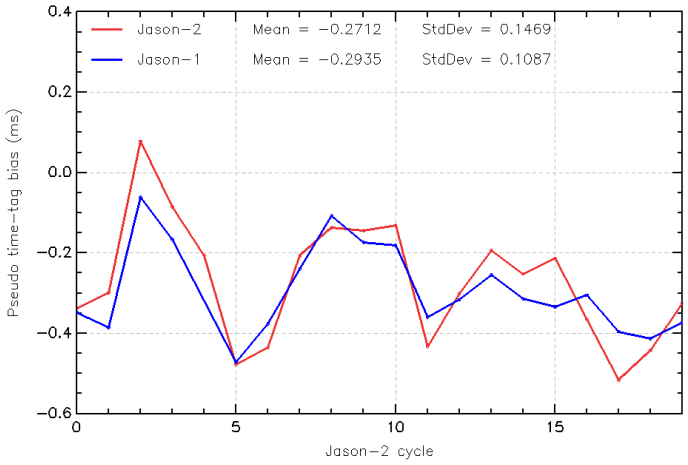

Figure 43: *Monitoring of pseudo time-tag bias estimated cycle by cycle from IGDR prodcuts for Jason-2 and Jason-1*

6. Sea Level Anomalies (SLA) Along-track analysis

6.1. Overview

The Sea Level Anomalies are computed along track from the SSH minus the mean sea surface (MSS) with the SSH calculated as defined in previous section 5.1. :

$$SLA = SSH - MSS(CLS2001)$$

As for the SSH crossovers, the SLA analysis is a complementary indicator to estimate the altimeter system performances. On the one hand, it allows to monitor the evolution of the global mean of the SLA, usually called Mean Sea Level (MSL). As it is a main indicator for climatic warming studies, the detection of jump or abnormal trend in the evolution of the MSL is an important item of Cal/Val activities. On the other hand, the SLA variability analysis in space and time is able to detect change in the altimeter system due to evolution in the product standards or due to an anomaly in the system.
As already described previously, the Jason-2 verification phase with Jason-1 allows us to compare both system accurately (since they use the same ground-track, spaced out by 55s). Thus they have to measure the same sea surface height. This is especially true for the SLA along-track analysis, since direct SLA comparisons are possible. In addition, it is not necessary to apply geophysical corrections for both SSH since it is theoretically the same. Finally, the SLA comparison between both missions gives directly information on the altimeter range and the orbit calulation differences. However, as the repetivity of both ground passes is not exact (± 1 kms), SLA measurements have to be projected and interpolated over the Jason/TOPEX theoretical ground pass ($\bar{T}$) in order to be compared. MSS have to be applied to take into account its cross-track variations.

$$\Delta SLA_{J1-J2} = [(Range_{Ku} - Orbite - MSS)_{J1}]_{\bar{T}} - [(Range_{Ku} - Orbite - MSS)_{J2}]_{\bar{T}}$$

Then in order to take advantage of the Jason-2 verification phase, we mainly focus in this chapter on the along-track SLA differences between Jason-1 and Jason-2 using POE and MOE orbit.

6.2. Mean of SLA differences between Jason-2 and Jason-1

6.2.1. Maps averaged per boxes

The map of SLA differences (averaged per boxes) between both missions have been calculated over all the Jason-2 period using alternatively MOE and POE orbits (see figure 44). Significant patches between ± 2 cm are observed with the MOE orbit on the left chart. In the meantime, the use of the POE orbit in SLA calulation reduces significantly this geographically correlated biases on the right chart. However a weak hemispheric signal is still observed between ± 0.5 cm.
The cycle by cycle SLA differences with the MOE are not stable and can reach ± 5 cm for some cycles. The figure 45 has been plotted calculating the temporal standard deviation of mean SLA differences using successively the MOE orbit on the left and the POE orbit on the right. These maps show the better stability of cycle by cycle SLA differences using the POE orbit (between 0.5 and 0.7 cm rms) than using the MOE orbit (between 1.2 and 1.4 cm rms with stronger pass effects).

In fact, these significant differences observed using MOE orbit are mainly due to the CNES Jason-1 MOE calculation. On the one hand, the comparison with Envisat SLA is in better agreement with Jason-2 SLA than Jason-1. Indeed, the SLA difference patches observed between Envisat and Jason-1 (see Envisat annual report, 2008 [7]) are well correlated with those observed between Jason-2 and Jason-1. On the other hand, other MOE orbit solutions (coming from GSFC) reduce signifivantly these effects (see in annex the poster 64 presented at the last OSTST, Nice, November 2008).

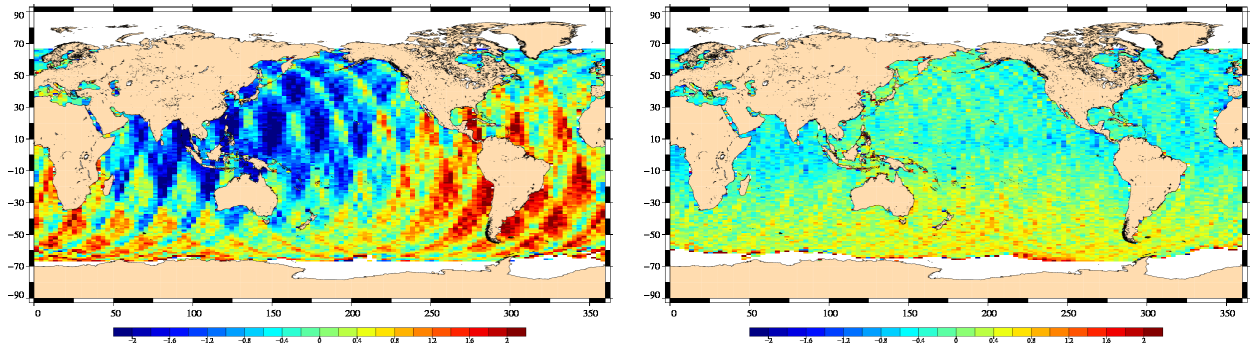

Figure 44: *Maps of SLA mean differences between Jason-1 and Jason-2 overall the period using MOE orbit (left) and POE orbit (right)*

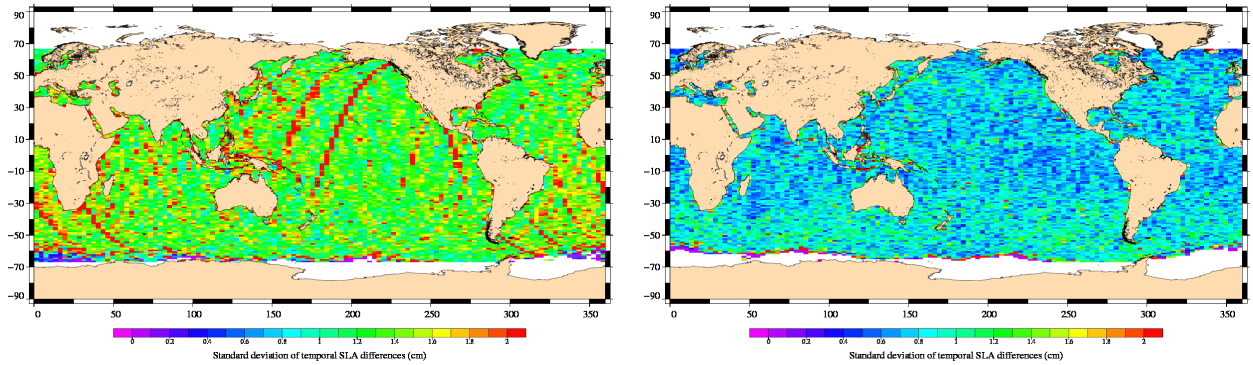

Figure 45: *Temporal standard deviation of SLA mean differences between Jason-1 and Jason-2 overall the period using MOE orbit (left) and POE orbit (right)*

6.2.2. Cycle by cycle monitoring

The global SSH bias between both missions is monitored on a cyclic basis since the beginning of Jason-2 in figure 46. On the left chart, the SSH bias (Jason-2 - Jason-1) is calculated using the MOE orbit applying and without applied the SSH corrections. The bias is respectively 8.3 cm and 8.0 cm with in both cases a good stability close to 0.15 cm rms. This bias is unchanged using the POE orbit in the SSH calculation as plotted on the right chart.
In order to determine the temporal stability of SLA differences, we calculated the mean and especially the standard deviation of cyle by cycle maps of SLA differences between Jason-1 and Jason-2 (see figure 47). This criteria brings out the importance to cumulate enough cycles to reduce the cycle by cycle effects between both missions. Using less than 10 cycles, the global SSH bias has stabilized around 7.9 cm and spatial SSH consistency is close to 1.2 cm rms with the MOE orbit and lower than 0.7 cm with the POE orbit. Similar statistics between Jason-1 and T/P are superimposed on the right chart using old altimetric standards (2003) and actual standards for T/P. The spatial SSH consistency is similar comparing Jason-1/Jason-2 and Jason-1/TOPEX systems using new standards. On the other hand, statitics obtained in 2003 just after the end of the Jason-1 verification phase (using POE) are significantly higher. They are of the same order as Jason-1/Jason-2 statistics with MOE orbits. This is a good indicator of the improvements achieved within 5 years in the ground processing system.

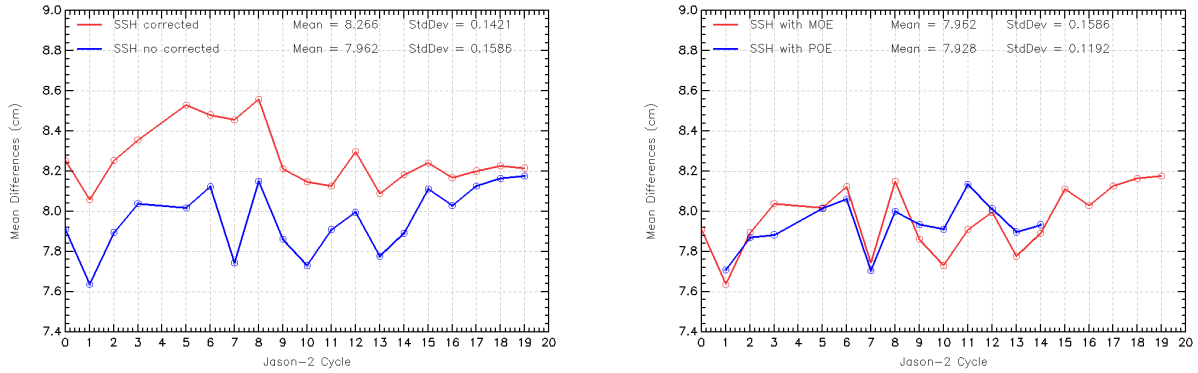

Figure 46: *Monitoring of global SLA bias (Jason-2 - Jason-1) correcting or not the SSH and using MOE orbit (on the left) and using MOE and POE orbit after correcting the SSH (on the right)*

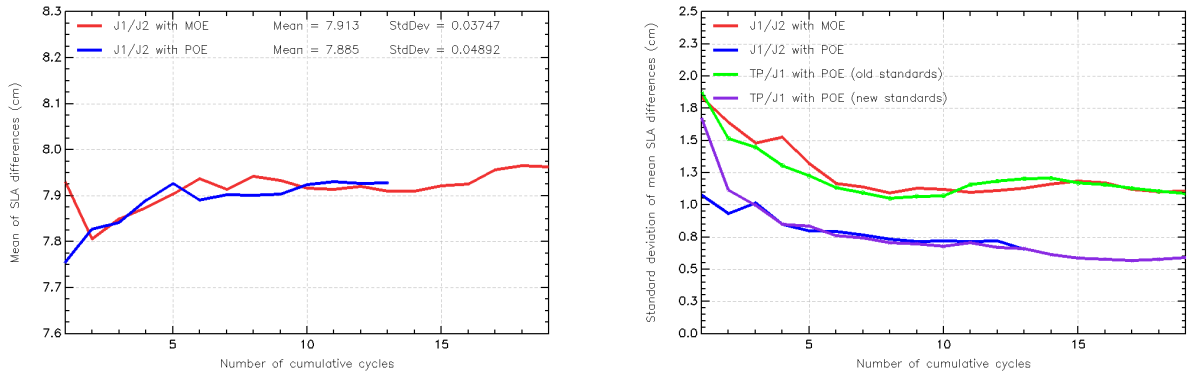

Figure 47: *Mean and the standard deviation evolution versus the cumulated cycle number of cycle by cycle maps of SLA differences between Jason-1 and Jason-2*

6.3. Standard deviation of SLA differences between Jason-2 and Jason-1

6.3.1. Maps averaged per boxes

The standard deviation of SLA difference is plotted in figure 48 using the MOE orbit on the left chart and the POE orbit on the right chart. As expected, standard deviation differences are mainly depending on the SWH values. This is explained by the 1-Hz SSH noise higher in strong SWH area due to the ground processing. Besides, no abnormal feature is displayed, showing the good consistency of both SLA between 3 and 5 cm RMS. Only some passes are displayed on the left chart due to inconsistency in MOE processing between both missions.

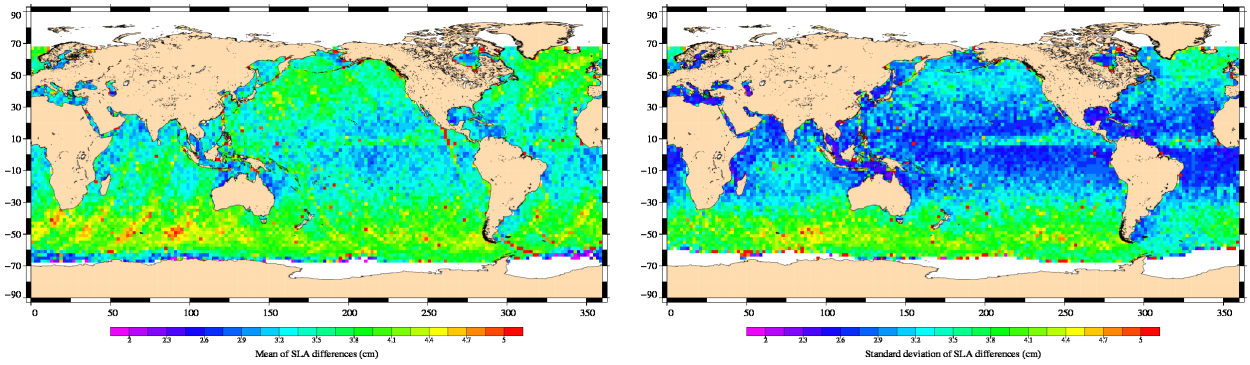

Figure 48: *SLA variance differences between Jason-1 and Jason-2 overall the period using MOE orbit (left) annd POE orbit (right)*

6.3.2. Cycle by cycle monitoring

The cycle by cycle monitoring of the global SLA differences standard deviation (plotted in figure 49) is very stable and weak over all the Jason-2 period. The average statistic is close to 3.9 cm rms using MOE orbits and 3.5 cm RMS using POE orbits.

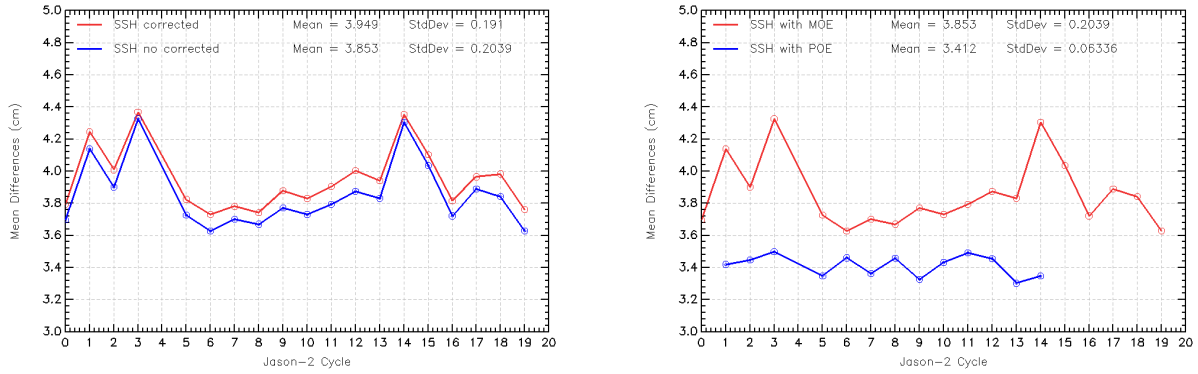

Figure 49: *Monitoring of the global standard deviation of Jason-1 and Jason-2 SLA differences correcting or not the SSH and using MOE orbit (on the left) and using MOE and POE orbit after correcting the SSH (on the right)*

6.4. SLA variance differences between Jason-2 and Jason-1

Maps of SLA variance differences have been calculated (figure 50) between Jason-2 and Jason-1 using alternatively the MOE (left chart) and POE orbits (right chart). Positive patterns (red on the maps) show areas where the Jason-2 variance is weaker than Jason-1 one. The better Jason-2 SLA performances calculated from the MOE (left chart) is well highlighted thanks to this basic criteria. Using the POE orbit, SLA variance differences are weak except in high oceanic variability areas. Though both satellites are very close in space and time, they do not measure exactly the same ocean which might explain these variance differences.

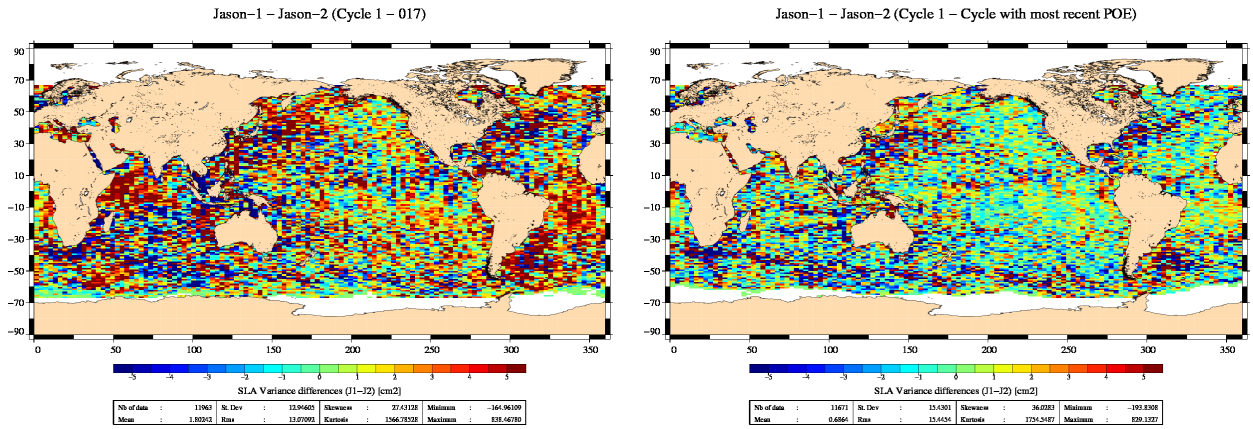

Figure 50: *SLA variance differences between Jason-2 and Jason-1 overall the period using MOE orbit (left) and POE orbit (right)*

7. Particular Investigations

This sections contains some investigations led on Jason-2 data, such as on the low signal tracking anomaly, on testing the use of MQE threshold for Jason-2 1 Hz compression and an analysis of high frequency spectrums.

7.1. Low signal tracking anomaly (AGC anomaly)

During SGT and also Median tracking mode, Jason-2 altimeter could track during several minutes low signal echoes with "Brown like" but "distorted" shape (see [4]). This concerned less than 0.5% of ocean measurements. An example of waveforms during such an anomaly is visible in [10]. This anomaly was especially noticeable over ocean. These measurements were edited by several parameters out of threshold: mispointing, backscattering coefficient, significant wave height. They also showed a drop in AGC (automatic gain control). These anomalies were called "low signal tracking anomaly" or "AGC anomaly". An example of low signal tracking anomaly is shown in figure 51.

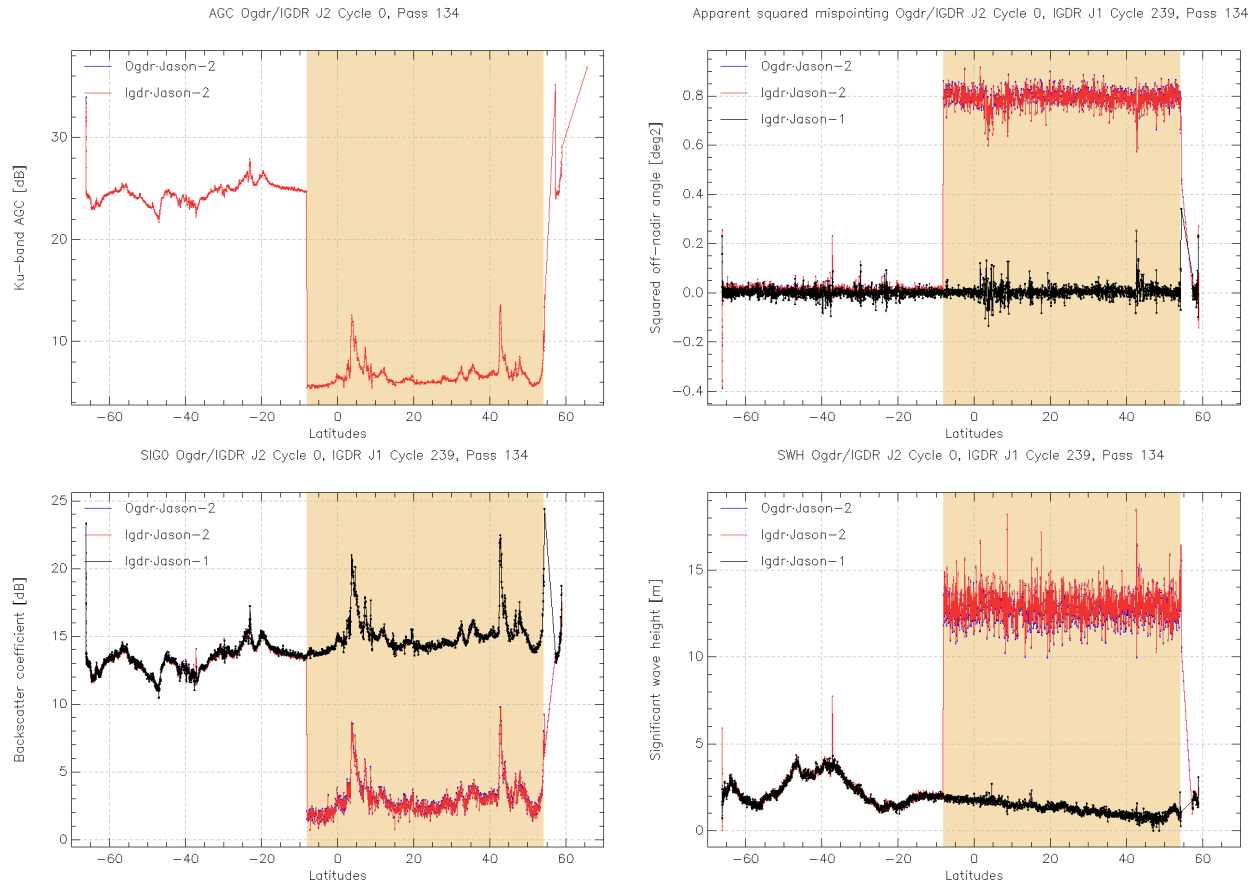

Figure 51: *Example of low signal tracking anomaly for pass 134, Jason-2 cycle 0. Several parameters are shown: AGC (top left), apparent squared mispointing (top right), Sigma0 (bottom left), and SWH (bottom right). Period of anomaly colored.*

Low signal tracking anomaly were especially severe (several tens of minutes) during SGT mode, they were shorter in median mode (at worst a couple of minutes) and never appeared during DEM modes. During cycle 16, on 10th of December, a correction for the low signal tracking anomaly (AGC anomaly) was uploaded (during pass 73). Till cycle 16, pass 70 AGC anomalies were still detected, biggest one (lasting approximately 2 minutes) on the transition Africa/ Indian ocean (pass 5). But no further AGC anomaly (on ocean) has occurred since the upload of the correction. The correction for the low signal tracking anomaly consists in more strict criteria for acquisition (to avoid that low signal echoes are tracked). This has no impact for the quantity of ocean measurements as shown on figure 52 where cycle 15 (before upload of correction for low signal tracking anomaly) and 18 (after upload of correction) show equivalent number of measurements. But number of tracked measurements over land has decreased (see figure 53 and 54).

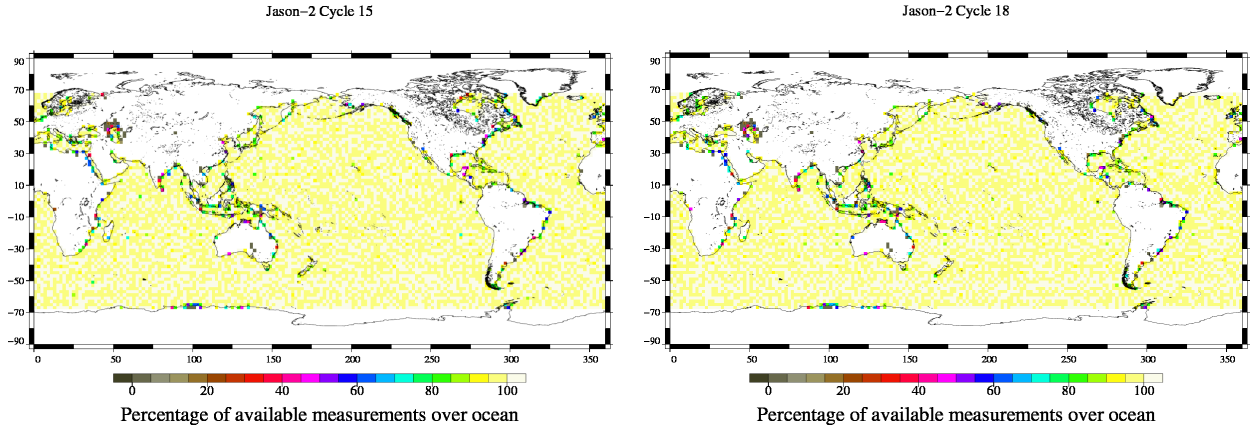

Figure 52: *Percentage of available measurements over ocean for Jason-2 cycle 15 (left) and 18 (right).*

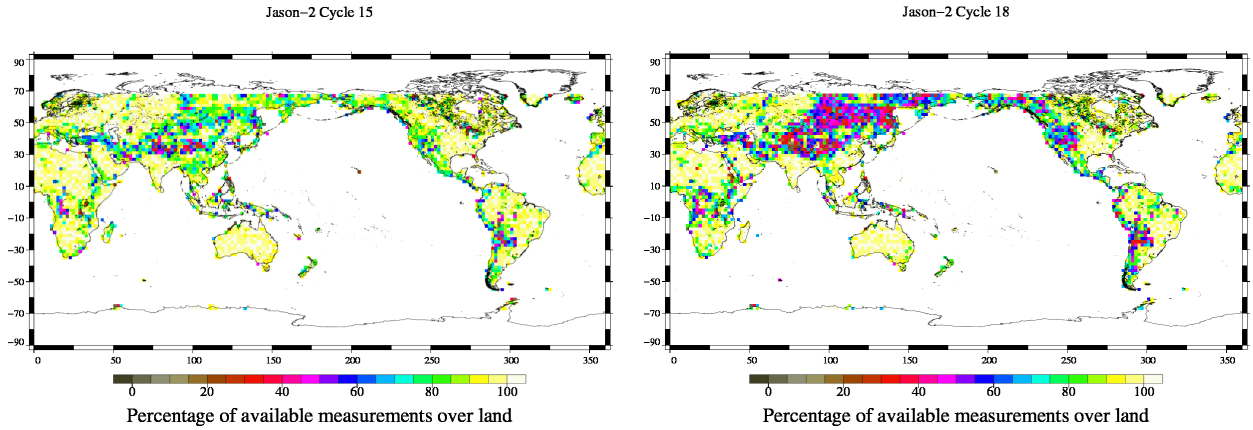

Figure 53: *Percentage of available measurements over land for Jason-2 cycle 15 (left) and 18 (right).*

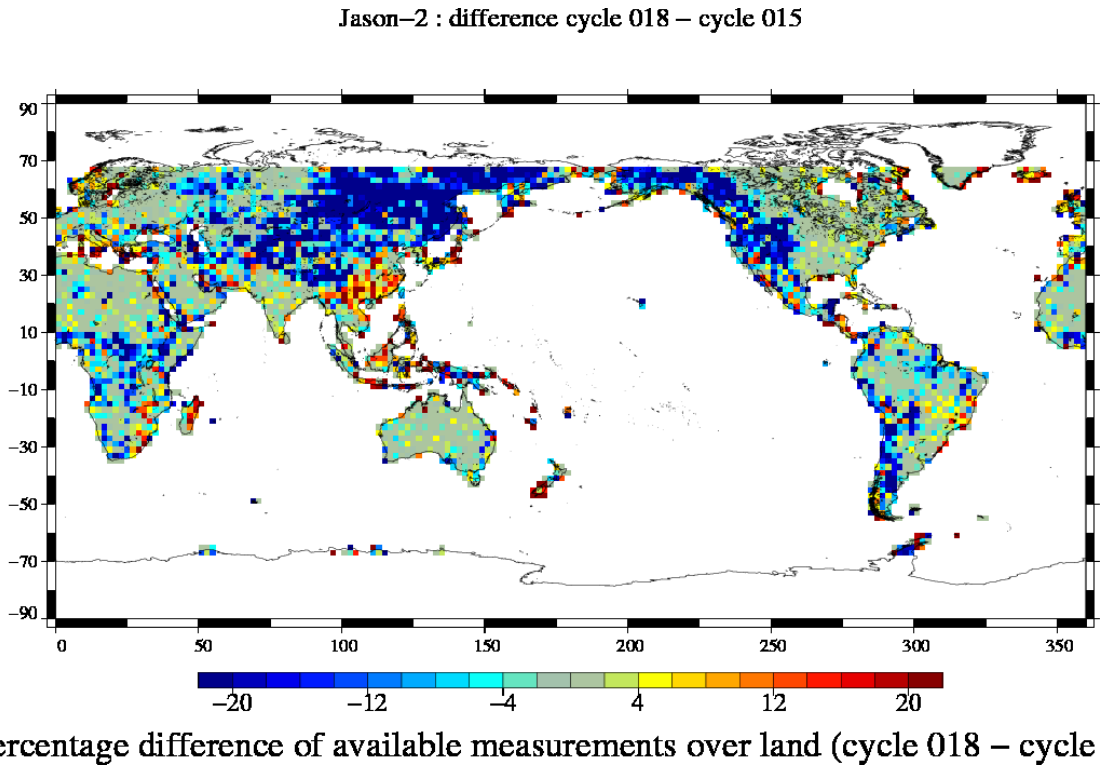

Figure 54: *Percentage difference of available measurements over land for Jason-2. Cycle 018 (after correction) - cycle 015 (before correction).*

7.2. Study applying MQE threshold during 1 Hz compression

Comparison maps of Jason-1 and Jason-2 differences (after interpolation on theoretical track) have shown regional differences around Indonesia especially for C-band parameters (number of elementary range measurements (figure 23, significant wave height (figure 28)), which seems to be correlated with MQE (Mean quadratic error) values (figure 55).

This is supposed to be due to the fact that for Jason-2 1-Hz compression, no threshold is used on MQE. This choice was made, since threshold from Jason-1 was not applicable to Jason-2 (it eliminated too much measurements).

This hypothesis was verified for Jason-2 Igdr cycle 10 by a study, using the following thresholds for MQE during compression : 0.0171 for Ku-band, and 0.1559 for C-band. These values correspond to 3 sigma (see figure 56).
The following parameters were therefore recomputed for Ku- and C-band: range, number and rms of elementary range measurements, significant wave height, rms of 20 Hz significant wave height measurements, backscattering coefficient, number and rms of 20 Hz backscattering coefficient. Dual-frequency ionospheric correction was recomputed using new range and (old) sea state bias.
Only a simple editing procedure was used, based on threshold editing, to keep valid measurements.

7.2.1. Comparison residus differences

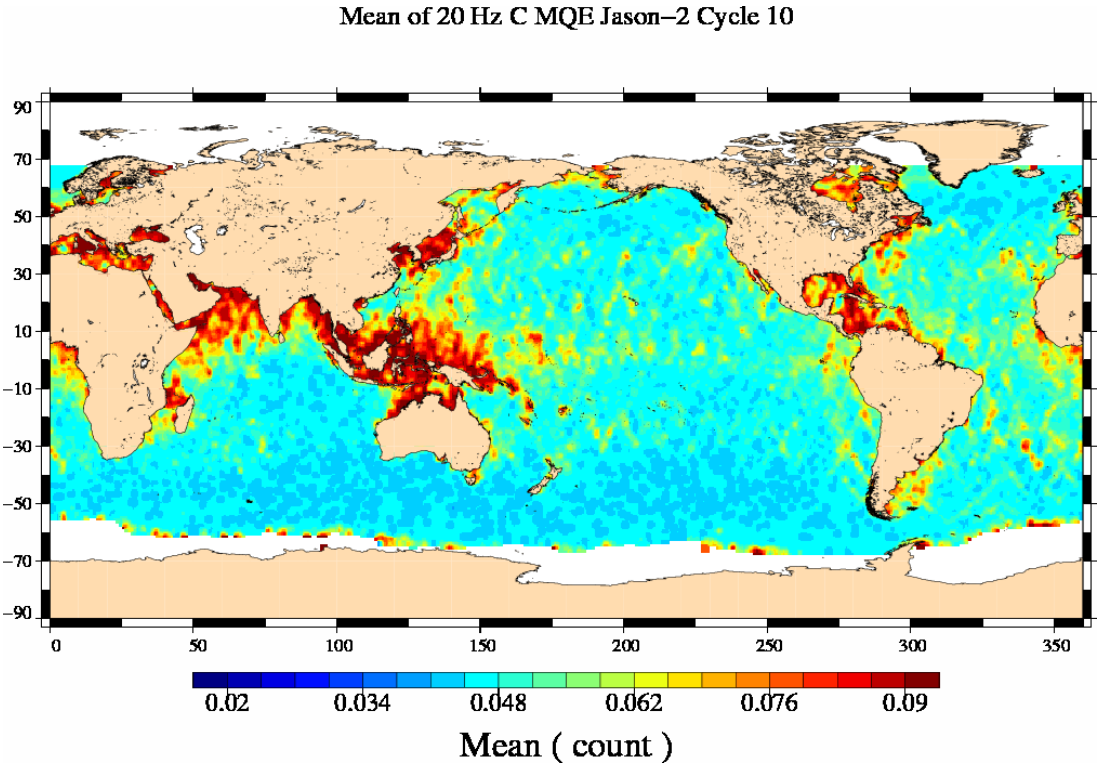

Figure 55: *Map showing C-Band MQE for Jason-2 cycle 10.*

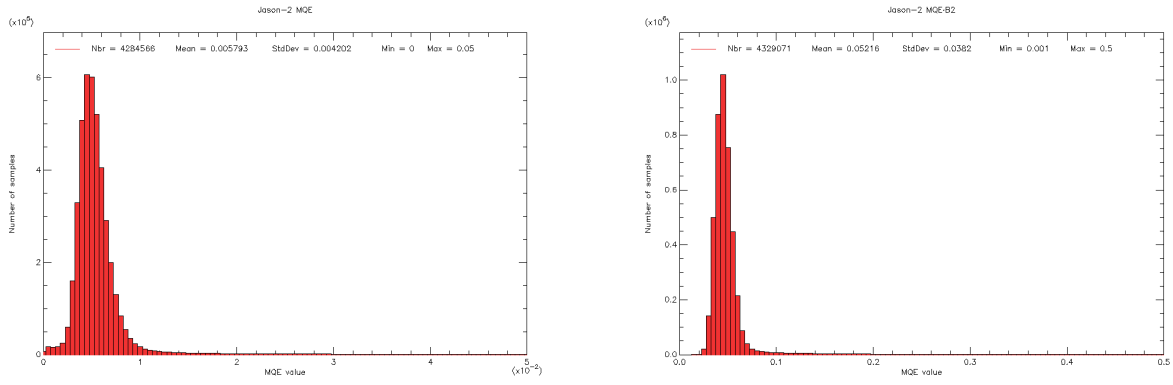

Figure 56: *Histogram of Jason-2 MQE for Ku-band (left) and C-band (right).*

In the following, residus differences (JA1-JA2) are shown for Jason-2 cycle 10 (Jason-1 cycle 249). These are differences of Jason-1 and Jason-2 measurements after interpolation on theoretical ground pass (as real ground passes of both satellites may deviate up to ±1km from theoretical ground pass). On the left side figures difference is made using variables from original Jason-2 products. On the right side Jason-2 variables were recomputed using the MQE threshold.

7.2.1.1. Ku - C band range difference

MQE threshold changes only slightly the bias of Ku - C-band range differences between Jason-1 and Jason-2. It goes from -4.75 cm (without MQE threshold) to -4.60 cm (with MQE threshold).

Nevertheless the differences visible in Mediterranean Sea, around Indonesia and in the Gulf of Mexico seem to be attenuated.

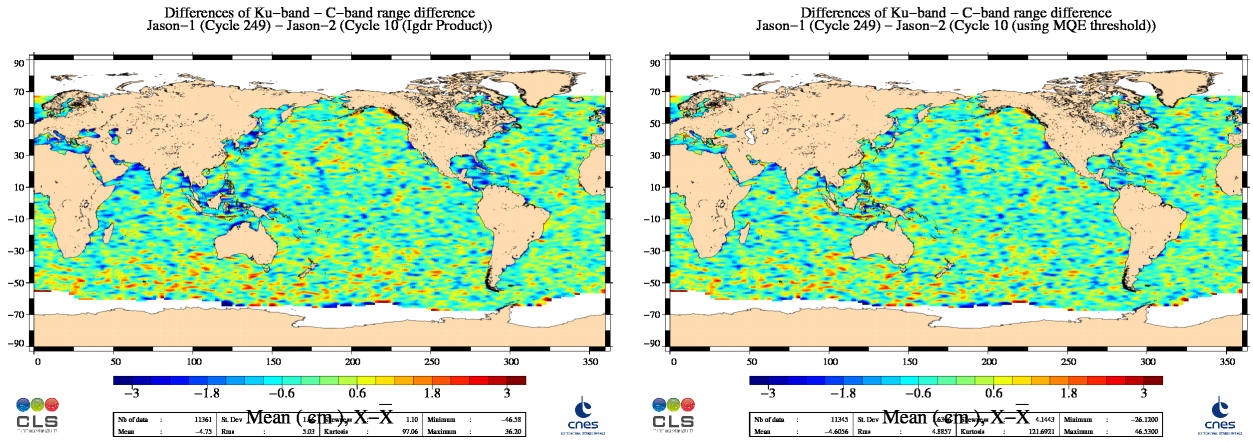

Figure 57: *Map showing mean of JA1-JA2 residus difference of Ku-band - C-band range difference. Left: original JA2 product, right recomputed JA2.*

7.2.1.2. Number of elementary C-band range measurements

Comparing elementary number of 20Hz C-band range measurements showed a mean bias of 0.2 counts, meaning that number of 20Hz C-band range measurements are in average lower for Jason-1 than for Jason-2, as some elementary measurements were eliminated by MQE threshold criterion active for Jason-1. Differences are especially visible for regions with high MQE values, as Mediterranean Sea and around Indonesia (left side of figure 58). Using also a MQE threshold for Jason-2, eliminates elementary 20 Hz C-band range measurements for Jason-2, so in average between the two satellites there is only a difference of 0.02 count. The large differences in high MQE regions have also disappeared (right side of figure 58).

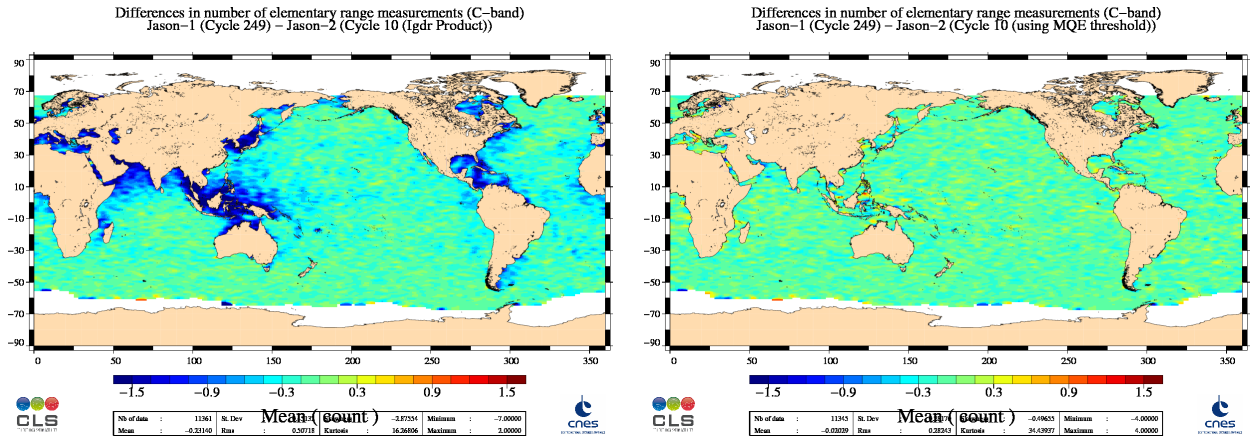

Figure 58: *Map showing mean of JA1-JA2 residus difference of number of elementary C-band range measurements. Left: original JA2 product, right recomputed JA2.*

7.2.1.3. C-band significant wave height

Using MQE threshold for Jason-2 increases the global bias of C-band SWH between Jason-1 and Jason-2 from -0.8 cm to -3.5 cm, but local biases are reduced.

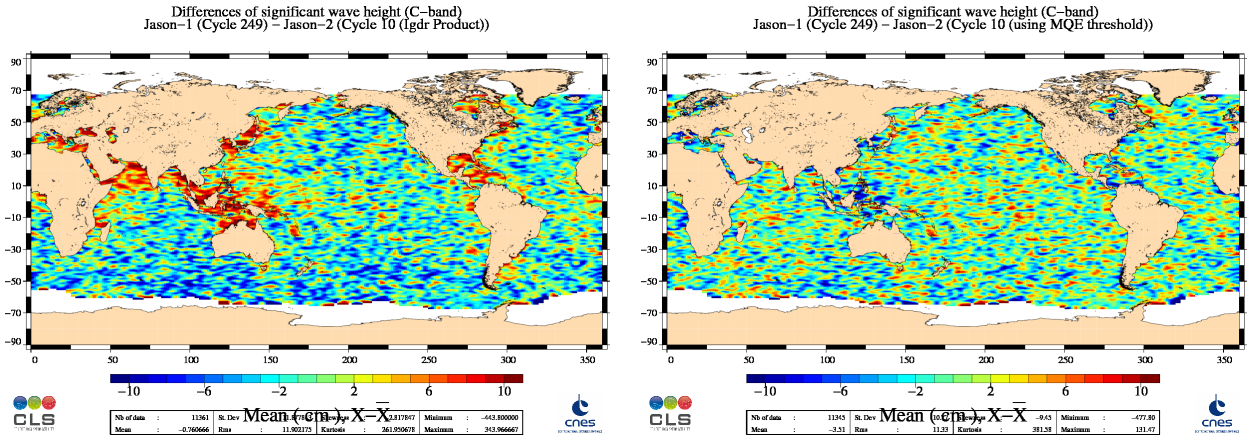

Figure 59: *Map showing mean of JA1-JA2 residus difference of C-band significant wave height. Left: original JA2 product, right recomputed JA2.*

The following table reminds the value around which the maps are centered.

parameter	JA1-JA2 mean (product)	JA1-JA2 mean (JA2 recomputed)
SWH Ku	-1.36 cm	-1.521 cm
SWH C	-0.760 cm	-3.51 cm
Rms of 20 Hz SWH Ku	0.146 cm	0.149 cm
Rms of 20 Hz SWH C	0.809 cm	0.803 cm
Rms of 20hz Ku range	-0.011 cm	-0.006 cm
Rms of 20hz C range	-0.003 cm	0.031 cm
Nb of 20hz Ku range	-0.117	-0.088
Nb of 20hz C range	-0.231	-0.020
altimeter ionosphere	-0.860	-0.835

7.2.2. Conclusion

The lack of MQE threshold on Jason-2 explains the local differences visible in Jason-1 - Jason-2 residus differences for number of elementary C-band range and C-band significant wave height.

7.3. High frequency content of Jason-2

Comparing the high frequency content of several missions enables to compare the performances but also to better understand the physical content of each signal. The spectral analysis allows to quantify accurately the global SSH HF for 1Hz and 20Hz data. Comparison are performed for Envisat and Jason-1 GDR data and Jason-2 IGDR data. Main results from this study [8] are shown here.

Analysis is based on the spectrogram method which consists in averaging N Fast Fourier Transform, calculated on samples constituted of M points along track. The length of the samples is 300 points or 15 seconds for 20Hz data and 160 seconds for the 1Hz data.
The SLA linear combinaison used is recalled here: SLA is a difference of Orbit, Range, Corrections and Mean Sea Surface (MSS) :

$$SLA = Orbit - Range - MSS - Corrections \tag{1}$$

Where the sum of correction is:

$$\begin{aligned} Corrections = {} & ssb.cls + iono.smooth + dry\_tropo.ecmwf + wet\_tropo.ecmwf\_G + inv\_baro.mog2d \\ & + ocean\_tide.got00V2\_S1\_S2 + solid\_tide + pole\_tide \end{aligned} \tag{2}$$

7.3.1. Envisat/Jason-1/Jason-2 1Hz spectrums

The 1Hz spectrums are computed from 10 days of data. High frequency content is compared for Jason-1, Envisat, and concerning Jason-2 using two tracker modes: Median and DEM (Digital Elevation Model). The shape of the high frequency content is, as expected very similar for the three missions. When using uncorrected SSH, Envisat SSH is slightly above the others in terms of noise (figure 60 left). This effect is cancelled when the SSH is corrected from instrumental and geophysical corrections and the spectrums of the three missions are superimposed (figure 60 right). Choice of tracking mode of Jason-2 has no impact on 1Hz spectrum, since whatever type of tracker used, the spectrums are similar.

7.3.2. Envisat/Jason-1/Jason-2 20Hz spectrums

Though the same SLA linear combinaison was used for the different missions (see further definition) and Jason-1 and Jason-2 are both POSEIDON altimeters, differences are visible on 20 Hz spectrums. Indeed, Jason-2 20 Hz high frequency noise shows a slight coloration when compared to other missions (see figure 61). By isolating one by one the differences of processing between Jason-1 and Jason-2, the origin of such unexpected coloration is analsed. Up to now, the following differences were listed:

- On Jason-2, three tracking modes are available: SGT, Median and DEM whereas the sole SGT is available on Jason-1.
- Both retracking are MLE4, applied on raw waveforms for Jason-2 and on compressed/uncompressed waveforms for Jason-1.

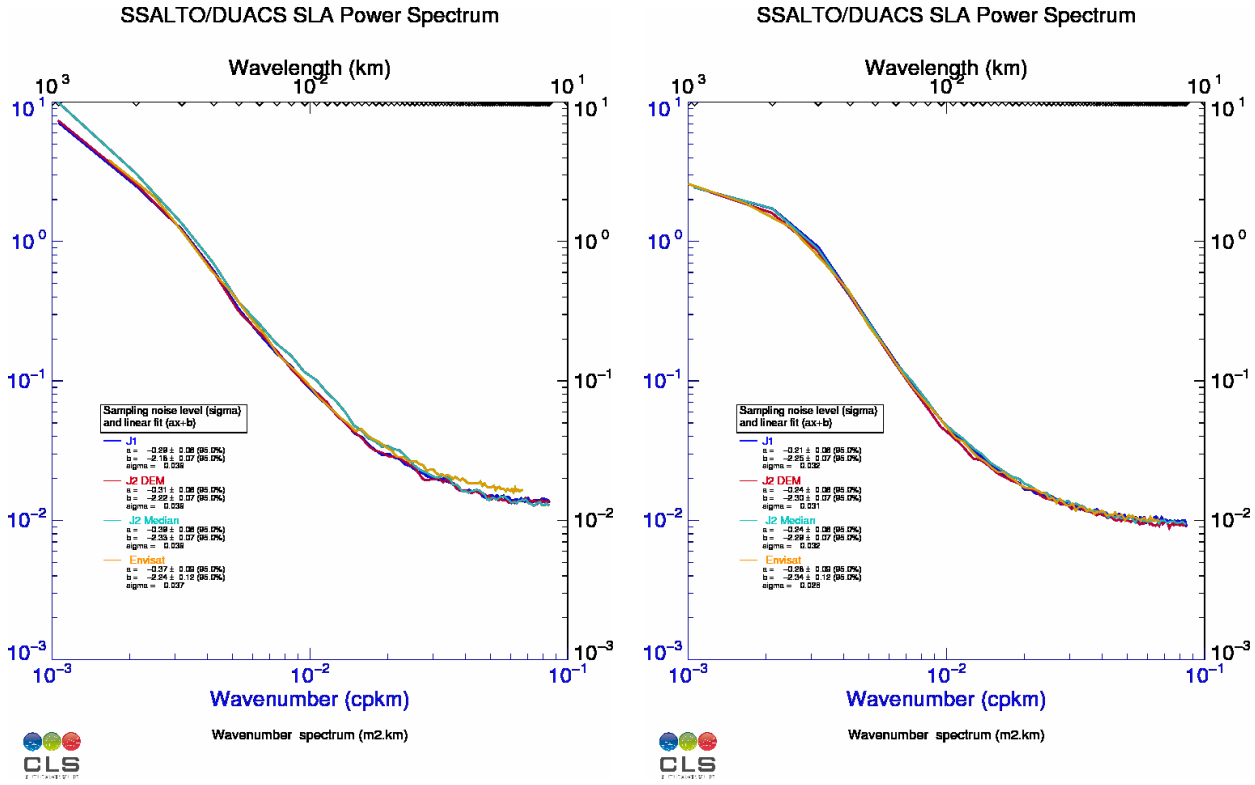

Figure 60: *1Hz spectrums versus km for the missions Envisat (yellow curve), Jason-1 (dark blue curve) and Jason-2 Median tracker mode (light blue curve) and DEM tracker mode (red curve) on Uncorrected data (left) and corrected data (right). Selection applied: Ocean validity and Latitude lower than 66 deg.*

- After the retracking a selection is applied on data to avoid too high MQE on Jason-1 whereas it is not done for Jason-2.
- The MOE orbit is used for Jason-2 IGDR data whereas POE orbit is used for Jason-2 IGDR data. This was also tested although orbit signs at very low frequency compared to this study's concerns.

20Hz spectrums are computed from 1 day of data. They are presented versus km for 10% missing points allowed and on uncorrected data. The minimum selection applied concerns the Ocean validity and Latitude lower than 66 deg. Further selections can be added for impact studies.

On 20Hz data, at frequencies higher than 3Hz, the Envisat signal is hidden by a plateau at 10-3m2s. This plateau is the signature of a 9.2 cm white noise. Assuming uncorrelated 20 Hz noise, it is equivalent to 2.1 cm for the 1 Hz averages. The Jason-1 spectra has a similar shape as Envisat but with a lower plateau (7.9cm).
On Jason-2, the spectrum does not behave as a white noise. A weak slope is noticed for the frequencies higher than 3Hz, showing a coloration on the noise at these frequencies. This effect is seen for all the tracker modes including SGT one (chosen for Jason-2's cycle 0 and half of cycle 1) which is identical to the one used on Jason-1. This different behavior is currently under investigations. By now, it was seen to be unchanged by selections on data (distance to coast, 20 valid data per second, selection on mispointing, waves or MQE criteria). Elsewhere, the spectrum is similar to

the other missions. Note that a higher energy in the 0.1-0.4 Hz (20-50km) bandwidth is noticed for the three missions.

Jason-2 noise is slighly correlated compared to Jason-1's (see 61 (left)).
Extensive studies were carried out to check that this :

- does not come from the tracker : even with the same SGT tracker as for Jason-1, the coloration persists (see 61 (right)).
- does not come from the selection applied on data : even with the same selection on the MQE as for Jason-1, the coloration persists (not shown see [8]).
- does not come from the step of compression/decompression applied on Jason-1's last samples of the waveforms before retracking : even with the same selection on the MQE as for Jason-1, the coloration persists (not shown, see [8]).
- is visible on the other parameters of the retracking (SIGMA 0) (not shown, see [8]).

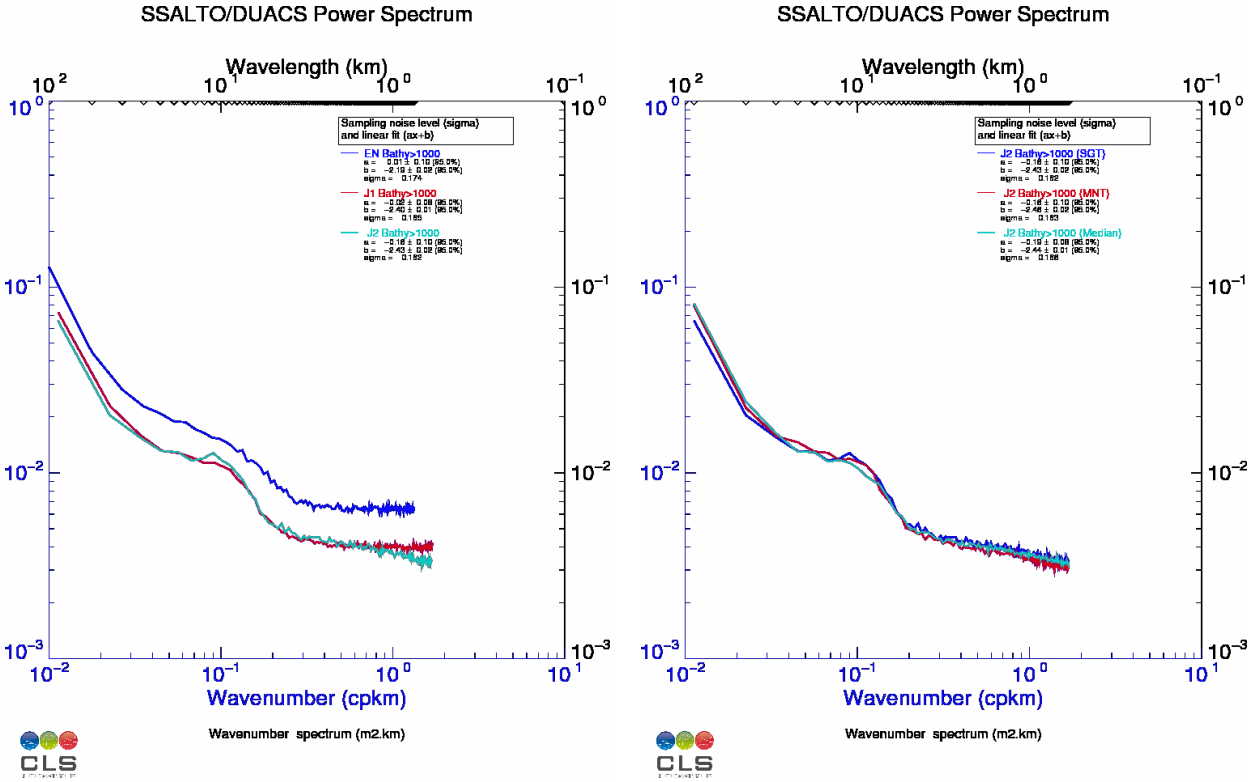

Figure 61: *20Hz spectrums versus km for the missions Envisat (dark blue curve), Jason-1 (red curve) and Jason-2 (ligh blue curve) (left). 20Hz spectrums versus km for the three Jason-2's tracker modes: SGT (similar to Jason) (dark blue curve), DEM (red curve) and Median (ligh blue curve).* ***Jason-2 noise is slightly correlated (slope of the noise plateau) for the 3 tracker modes.***

7.3.3. Conclusion

At 1Hz, the three missions Envisat, Jason-1 and Jason-2 compared have a complete agreement as long as the corrected SLA is considered.
On the other hand, an unexplained coloration of the noise above 3Hz is noticed for Jason-2. This coloration is particularly evidenced when the spectrum is compared to other missions' spectrums (here Jason-1 and Envisat) who present a white noise at these frequency, consistently to the theory. By now all the identified differences of processing between Jason-1 and Jason-2 were tested to see if they could explain this unexpected difference. But, apparently, this coloration does not come from :
- the new Jason-2's tracking modes
- the step of waveforms' compression/uncompression step for Jason-1
- the MQE selection applied after the retracking on Jason-1

Furthermore, the effect was seen to be visible on other parameters as the SLA, which would remove the possiblity of a difference in the SLA's linear combinaison.

This coloration on high frequency Jason-2's data remains unexplained.

8. Conclusion

Jason-2 is in orbit since 20th of June, 2008 flying during the verification phase in tandem with Jason-1 (55s apart) over the same historical TOPEX/Poseidon ground track (till cycle 20). This allows extensive verification and validation of the data, as both satellites observe the same geophysical phenomena. OGDR and IGDR data quality was already approved during OSTST 2008 meeting in Nice. OGDR products are distributed to users since mid-December 2008 and IGDR since mid-January 2009. In addition, the GDR production started end of February 2009 (restricted to PIs).

The verification phase has shown that Jason-2 data quality is excellent, at least of the same order as the Jason-1 one. The raw data coverage is similar to Jason-1's over ocean and improved in coastal areas. Thanks to the new altimeter tracking modes, the availability of land measurements is significantly improved. Over ocean, the valid data coverage is similar since the additional Jason-2 raw measurements are removed by the editing procedure. But thanks to studies on going (in PISTACH ans SLOOP projects), we can benefit from these new measurements to calculate the SSH especially in coastal areas and over the rivers and lakes.

The altimetric parameter analysis has shown a similar behavior compared to Jason-1. Some biases exist as between dual-frequency ionosphere correction, but they are stable. However, they are not yet completly understood and will have to be explained. All these parameters will be unchanged between IGDR and GDR. Though Advanced Jason-2 radiometer performances are improved especially near coasts, potential stability problems are observed in Jason-2 IGDR product (small jumps (versus JMR) occurred in 34 GHz channel). These potential stability problems are thought to be corrected thanks to new ARCS system applied for GDR.

The SSH performances analyzed at crossovers or along-track highlight similar performances between Jason-1 and Jason-2 using the preliminary CNES POE orbits (before the official GDR production). The consistency between both SLA is remarkable with a small hemispheric signal lower than 0.5 cm. This signal is removed using GSFC orbits proving the sensibility of the orbit calculation for the detection of geographically correlated biases. In addition, the SLA comparison between both missions using MOE orbits reveals some systematic differences with SSH biases between $\pm$ 5 cm varying in time. In fact, they are due to the MOE Jason-1. Finally, using OGDR product, a dramatic improvement is observed with Jason-2 thanks to the DIODE orbit. The OGDR product performances is now sufficient to be integrated directly in operational systems as DUACS for instance.

The verification phase between Jason-1 and Jason-2 allowed us to check accurately the Jason-2 mission. As during the Jason-1/TOPEX verification phase, we also learned a lot from Jason-1 measurement quality. To balance all these excellent results and especially the quasi-perfect SSH consistency between both missions (using POE orbit), both systems can contain similar errors undetectable with the analyzes performed here. Comparisons with external and independent datasets (Tide gauges, Temperature/Salinity profiles, ...) are thus essential to detect potential errors.

Given the very good Jason-2 data quality, the Jason-2 verification phase with Jason-1 ended on 26th of January. At this time, Jason-1 was moved to the interleaved ground track already used by TOPEX. Scientific studies and operational applications will very soon benefit from the combination

of Jason-2, Jason-1, and Envisat data.

9. References

References

[1] Brown G.S., "The average impulse response of a rough surface and its application", IEEE Transactions on Antenna and Propagation, Vol. AP 25, N1, pp. 67-74, Jan. 1977.

[2] Brown S., S. Desai, and W. Lu "Initial on-orbit performance assessment of the advanced microwave radiometer and performance of JMR GDR-C", Oral presentation at OSTST meeting, Nice, France, 9-12 november 2008. Available at http://www.aviso.oceanobs.com/fileadmin/documents/OSTST/2008/oral/brown_calval.pdf

[3] Chambers, D., P., J. Ries, T. Urban, and S. Hayes. 2002. Results of global intercomparison between TOPEX and Jason measurements and models. Paper presented at the Jason-1 and TOPEX/Poseidon Science Working Team Meeting, Biarritz (France), 10-12 June.

[4] Desjonqueres, J.-D., G. Carayon, J.-L. Courriere, and N. Steunou "POSEIDON-2 In-Flight results", Oral presentation at OSTST meeting, Nice, France, 9-12 november 2008. Available at http://www.aviso.oceanobs.com/fileadmin/documents/OSTST/2008/oral/desjonqueres.pdf

[5] Dumont, J.-P., V. Rosmorduc, N. Picot, S. Desai, H. Bonekamp, J. Figa, J. Lillibridge, R. Sharroo, 2008: OSTM/Jason-2 Products Handbook. CNES: SALP-MU-M-OP-15815-CN. EUMETSAT: EUM/OPS-JAS/MAN/08/0041. JPL: OSTM-29-1237. NOAA/NESDIS: Polar Series/OSTM J400. Available at http://www.aviso.oceanobs.com/fileadmin/documents/data/tools/hdbk_j2.pdf

[6] Le Traon, P.-Y., J. Stum, J. Dorandeu, P. Gaspar, and P. Vincent, 1994: Global statistical analysis of TOPEX and POSEIDON data. *J. Geophys. Res.,***99, 24619-24631.**

[7] Ollivier A., Faugere Y., Granier N., 2008: Envisat RA-2/MWR ocean data validation and cross-calibration activities. Yearly report. Technical Note CLS.DOS/NT/09.10, Contract N° SALP-RP-MA-EA-21633-CLS http://www.aviso.oceanobs.com/fileadmin/documents/calval/validation_report/EN/annual_report_en_2008.pdf

[8] Ollivier A., Faugere Y., P. Thibaut, G. Dibarboure, and J.-C. Poisson, 2008: Investigation on the high frequency content of Jason-1 and Jason-2. CLS.DOS/NT/09-027

[9] Thibaut, P. O.Z. Zanifé, J.P. Dumont, J. Dorandeu, N. Picot, and P. Vincent, 2002. Data editing : The MQE criterion. Paper presented at the Jason-1 and TOPEX/Poseidon Science Working Team Meeting, New-Orleans (USA), 21-23 October.

[10] Thibaut, P., J.-C. Poisson, A. Ollivier, S. Philipps, and M. Ablain: "Jason-2 waveforms, tracking and retracking analysis", Oral presentation at OSTST meeting, Nice, France, 9-12 november 2008. Available at http://www.aviso.oceanobs.com/fileadmin/documents/OSTST/2008/oral/thibaut.pdf

10. Annex

This annex contains posters presented at OSTST meeting in 2008.

10.1. Poster presented at OSTST meeting 2008

The following posters, presented at OSTST meeting 2008 in Nice (France), are also available on Aviso web-site: http://www.aviso.oceanobs.com/en/courses/ostst/ostst-2008/index.html.

(A) GLOBAL Statistical Jason-2 assessment and cross-calibration with Jason-1

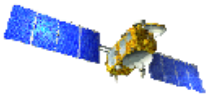

S.Philipps[1], M. Ablain[1], P.Thibaut[1], N.Picot[2]
[1]CLS, Space Oceanography Division, Toulouse, France
[2]CNES, Centre National d'Etudes Spatiales, Toulouse, France

Overview

The OSTM/Jason-2 (JA2) satellite was successfully launched on June, 20th 2008. Since July, 4th, Jason-2 is on its final orbit, flying in tandem with Jason-1 (JA1), only 55s apart. This poster assesses the JA2 data quality. Missing and edited measurements are monitored. Furthermore relevant parameters derived from instrumental measurements and geophysical corrections are analyzed. Analyzes are focused on JA1/JA2 cross-calibration since both missions are on the same orbit during the Calibration/Validation phase. This allows to precisely assess parameter discrepancies between both missions in order to detect geographically correlated biases, jumps or drifts. The SLA performances and consistency with JA1 are described in poster (B).

The study is conducted for JA2 cycles 0 to 10, corresponding to JA1 cycles 239 to 249. For both satellites IGDR (Interim Geophysical Data Records) 1 Hz data are used.

For Jason-2, two modes of on board tracking are used: Median tracker (for cycles 1,2,4,6,8,9,10,..) and Diode/DEM tracker (for cycles 3,5,7). Cycle 0 and half of cycle 1 was in SGT mode. Most of the following plots integrate all the cycles from 0 to 10. Indeed analysis of parameters obtained during cycles with different tracking modes does not reveal any particular behavior linked to the tracking mode.

Missing and Edited measurements

Over open ocean, JA2 and JA1 data coverage are very similar. Few missing measurements are however detected for Jason-2 over ocean, mostly due to station acquisition problems (cycle 001 pass 44-46, cycle 003 pass 33-34, cycle 005 pass 237-240) or ground processing anomalies (cycle 001 pass 145, cycle 005 pass 141). Note that from 7th to 20th of August 2008, no measurements are available for Jason-1, period for which the satellite was in safehold mode. Over coastal and hydrological zones, JA2 is much better than JA1 due to new tracker algorithms (Median and Diode/DEM).

For open ocean calval, the same editing procedure is applied for both satellites. Percentage of edited measurements is very similar, since approximately 16% (~12% due to ice flag and ~3% due to parameters out of thresholds) of ocean Jason-2 measurements are edited for each cycle. In Median mode, small portions of a pass are sometimes edited, due to AGC, Sigma0, waves and apparent mispointing out of threshold.

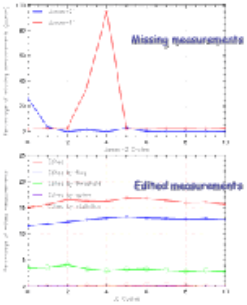

Backscattering coefficient

The JA2 backscattering coefficient (Sig0) shows good agreement with JA1 in Ku and C bands as plotted in map of mean differences (fig. 1) and in daily monitoring (fig. 2). The global bias with JA1 is weak (0.1 dB in Ku-band and 0.2 dB in C-band). In comparison, the global bias between JA1 and T/P was about 2.4 dB. Notice that a small signal (0.1 dB) in both Ku- and C-band differences is detected in daily monitoring (fig. 2).

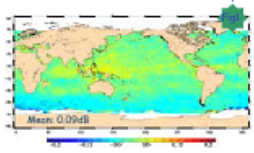

Map of JA1-JA2 Ku-band Sigma0 differences (mean over cycles 0 to 10) (fig. 1). Daily monitoring of mean and std of JA1 - JA2 Sig0 difference (fig. 2).

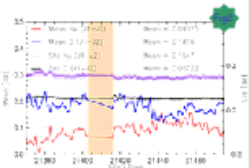

Significant Wave Height

The Significant Wave Height (SWH) shows very good agreement between JA2 and JA1 (fig. 10). Daily monitoring (fig. 11) of mean and std of JA1-JA2 SWH differences shows no drift neither for Ku-band nor for C-band. Waves between JA1 and JA2 are more coherent in Ku-band than in C-band. Mean of JA1-JA2 SWH differences are : -1 cm (Ku-band) and -0.2 cm (C-band). Std of JA1-JA2 SWH differences are : 17.5 cm (Ku-band) and 43.6 cm (C-band). Mean Ku-band SWH difference between T/P and JA1 was 8.9 cm. Weak regional differences around Indonesia (fig. 10) are very likely explained by the difference of MQE editing criteria used for both missions during 20 Hz to 1 Hz compression.

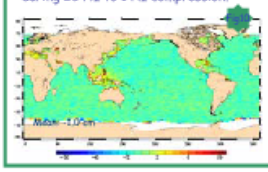

Map of JA1-JA2 Ku-band Sigma0 differences (mean over cycles 0 to 10) (fig.10). Daily monitoring of mean and std of JA1 - JA2 SWH difference (fig.11).

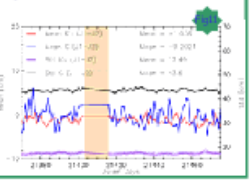

Wet troposphere correction

Difference of JMR - AMR radiometer wet troposphere correction (fig. 3) showed in the beginning of the mission a small drift (probably due to the heating of the instrument), during cycles 1 to 3, it was quite stable. After the Jason-1 safehold, difference shows a signal up to 7 mm amplitude. The reason is unknown, but caused by JMR (JA1), as visible on fig. 4 showing difference between radiometer and ECMWF model.

Towards the last cycles, a small drift seems to be visible, not only for JA1 and JA2, but also for Envisat, so this is probably due to the model. Behavior of JMR and AMR far away from coast is similar (fig.5), with AMR staying more stable than JMR when approaching coast related to different antenna properties.

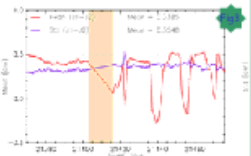

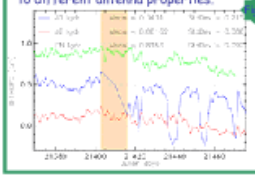

Daily monitoring of JA1-JA2 radiometer correction (fig.3). Mean of radiometer - model wet troposphere correction per day (fig.4) and in function of coast distance (fig.5).

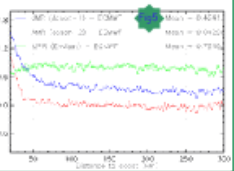

Apparent squared mispointing from waveforms

Daily monitoring of apparent squared mispointing from JA2 waveforms is much more stable than JA1 (see fig.12). This is due to reduced star tracker availability for JA1 which leads to a poorer pointing of the satellite. The JA2 satellite has no real mispointing, but mean value of apparent squared mispointing is around 0.0125 deg2 (0.11 deg), which is slightly higher than what is observed by the satellite teams.

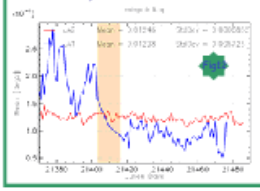

Daily monitoring of JA2 apparent squared mispointing (from waveforms) (fig. 12). Histogram showing JA1 and JA2 apparent squared mispointing for JA2 cycle 010 (fig. 13).

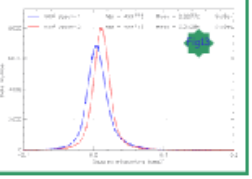

Number and Rms of 20 Hz elementary range measurements

Daily monitoring of JA1 - JA2 difference concerning the number of Ku and C-band 20 Hz elementary range measurements is very stable (fig. 6). Rms of 20 Hz elementary range measurements are equivalent for JA1 and JA2 (fig. 7).

Up to now, the MQE (Mean Quadratic Error between the measured waveform and the best fitted Brown model) is not used during the 20 Hz to 1 Hz compression. The number of elementary valid 20 Hz measurements per second is consequently higher for JA2 than for JA1.

Fig. 8 and 9 show, that this difference is mostly visible where the MQE is great ie where the waveforms (in C band) are corrupted.

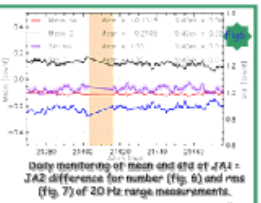

Daily monitoring of mean and std of JA1 - JA2 difference for number (fig. 6) and rms (fig. 7) of 20 Hz range measurements.

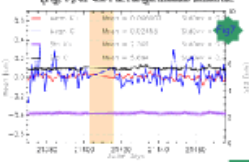

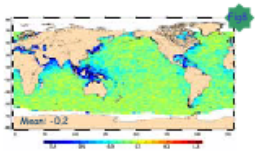

Difference map of JA1-JA2 number of elementary 20 hz C-band range measurements for JA2 cycle 010 (fig. 8), map of 20 hz C-band MQE (fig. 9).

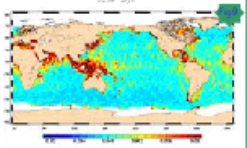

Altimeter ionospheric correction

The map of mean differences over cycles 0 to 10 (fig. 14) shows that altimeter ionospheric correction of JA1 and JA2 are in good agreement. Note that the global bias is -0.9 cm (under investigation), but it is stable (fig. 15) with small variations up to 2 mm from one day to another. As for other altimeter parameters, differences are slightly higher in some regions like Indonesia (probably MQE criteria).

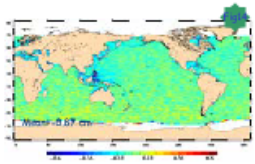

Map of JA1 - JA2 ionospheric correction, mean over cycles 0 to 10, except for cycle 4 (fig. 14). Daily monitoring of JA1-JA2 (filtered) altimeter ionospheric correction (fig. 15).

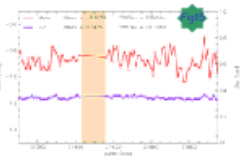

Conclusion

This study, using 11 cycles of Jason-2 flying in tandem with Jason-1, shows the very good consistency between altimetric parameters of JA1 and JA2.
Improvements are observed thanks to the JA2 radiometer (AMR), more stable than the JMR. Furthermore, the new JA2 DEM tracking mode (used during cycles 3, 5, and 7) shows no impact on parameter analysis of 1 Hz ocean measurements. The very small differences observed (principally in C-band) do not impact the SSH computation (see poster B). They are very likely due to the MQE editing which is not yet tuned for JA2 (under investigation).

Finally, from the Cal/Val parameter analysis point of view, additional JA2 cycles in tandem configuration are not necessary to better estimate on the one hand, the quality of Jason-2 parameters and on the other hand, the parameter consistency with Jason-1.

CLS Collecte Localisation Satellites
8-10 rue Hermes
31520 Ramonville Saint-Agne - France

OSTST
Nice, November 2008

cnes

Figure 62: *Poster presented at OSTST meeting, Nice 2008*

(B) Jason-2 and Jason-1 SLA Performances and Consistency

M. Ablain[1], S. Philipps[1], N.Picot[2]

[1]CLS, Space Oceanography Division, Toulouse, France
[2]CNES, Centre National d'Etudes Spatiales, Toulouse, France

Overview

This study aims at presenting the Jason-2 and Jason-1 SLA performances and consistency. On the one hand, SSH crossovers analyses provide the global performances of the Jason-2 system using OGDRs, IGDRs products and a preliminary Jason-2 POE orbit. Performances with similar Jason-1 statistics are compared. On the other hand, along-track analyses allow us to check the SLA consistency between both missions. Peculiar attention is paid on the global SSH bias and correlated geographically SSH bias using MOE and POE orbits.

Data used for Jason-1 and Jason-2		
Products	Jason-1	Jason-2
OGDRs	Cycles 239 to 249	Cycles 0 to 10
IGDRs	Cycles 239 to 249	Cycles 0 to 10
GDRs	Cycles 239 to 246	Preliminary POE updated in IGDRs data for cycles 1 to 7

Along track SLA analyses

Cycle by Cycle monitoring

The global SSH bias between Jason-2 minus Jason-1 is +8.3 +/- 0.2 cm using MOE or POE orbits for both satellites (Fig. 1), and without using any correction in SSH calculation. It is very stable with weak variations around 0.2 cm. Applying all the usual correction (not shown here), the bias is reduced close to 7.5 cm, mainly due to the altimeter ionospheric bias between Jason-1 and Jason-2.
The standard deviation of global SLA differences is also very stable and weak over all the Jason-2 period (fig.2) with figures close to 3.9 cm RMS using MOE orbits and 3.5 cm RMS using POE orbits.

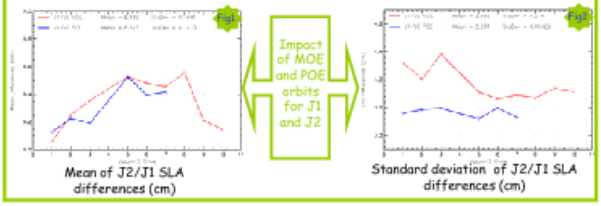

Spatial Analyses

The map of mean of Jason-1/Jason-2 SLA differences over all the period from IGDRs products highlight correlated geographical biases as plotted in figure 3, ranging between +/- 3 cm. As expected, these patches are almost completely removed using POE orbits (fig. 4), showing the very good consistency between both missions. However, very weak hemispheric structures remain with an amplitude close to 1 cm. They are very likely related to the orbit calculation. In addition, the structures observed using MOE orbit vary in space and in amplitude from one cycle to another as shown by the analyze of the temporal variability of the SLA differences (fig. 5). Using POE orbit, these variations are significantly reduced (fig. 6).

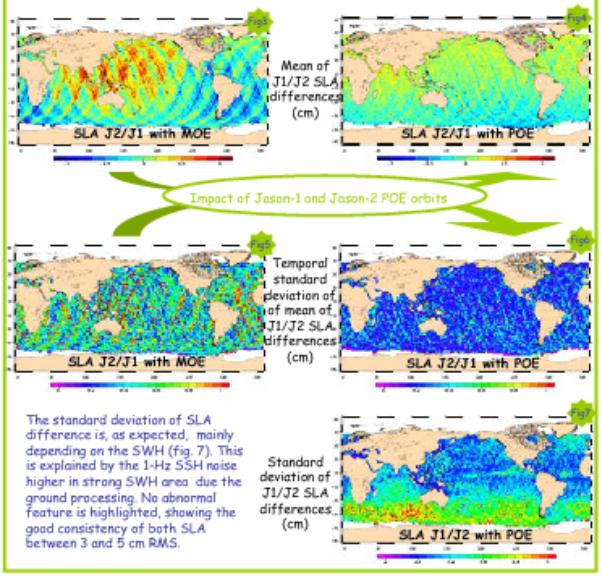

The standard deviation of SLA difference is, as expected, mainly depending on the SWH (fig. 7). This is explained by the 1-Hz SSH noise higher in strong SWH area due the ground processing. No abnormal feature is highlighted, showing the good consistency of both SLA between 3 and 5 cm RMS.

Comparisons with J1/TP SLA consistency during the Cal/Val phase

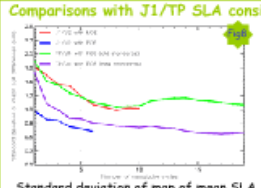

The standard deviation of map of mean SLA differences over a given period provides also a good criteria to measure the SLA consistency. Using 20 cumulative cycles (Jason-1 Cal/Val phase), the statistic forTP/J1 SLA differences was around 1.1 cm RMS with old standards (2002) and 0.6 cm RMS with new standards (2007). At the moment, J2/J1 differences using POE orbit provide a similar statistic but using only 6 cycles. In addition, applying MOE orbit, the statistic is in the same order as J1/TP one with old standards but with a POE orbit.

SSH Crossovers analyses

Cycle by Cycle monitoring

The monitoring of Jason-2 SSH statistics at crossovers are very good. A slightly improvement is observed using IGDRs in comparison with Jason-1 : SSH crossover mean is more stable (fig 1), and SSH crossover standard deviation is lower (5.5 cm RMS for J2 instead 5.7 cm RMS for J1 (fig.3)). Results is reversed comparing the GDRs products, but the Jason-2 's POE orbit is preliminary at the moment.
Concerning the OGDRs, a dramatic improvement is observed at SSH crossover mean (fig. 2) and standard deviation (fig. 4). This is explained by the better quality of Jason-2 DIODE orbit .

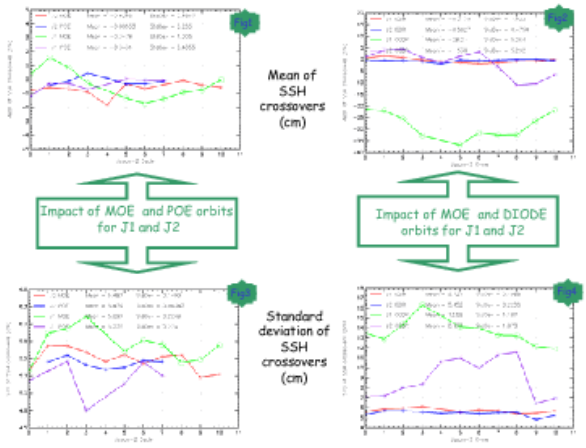

Spatial Analyses over all the period

The map (over all the period) of SSH crossovers mean is a little more homogeneous for Jason-2 (fig. 6) than for Jason-1 (fig.6) using IGDR products. Maps of SSH crossovers standard deviation are similar (fig. 7 and 8) between both missions, with RMS statistics slightly weaker for Jason-2 in weak oceanic variability areas. These both items bring out the very good quality of Jason-2 SSH in relationship with the quality of Jason-2 MOE orbit,.

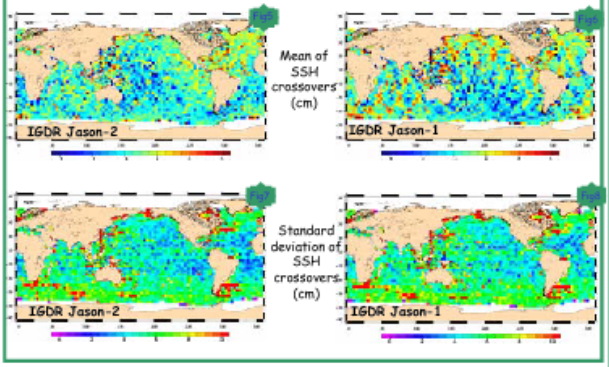

Conclusion

In this study, we show the good performances of Jason-2 SSH in the same order or better than Jason-1 ones. In addition, the SLA consistency between both missions is already very good just 4 months after the launch, in the same order as Jason-1/TP over all the verification phase. The weak remaining SLA differences observed by hemisphere using the POE orbits (around 1 cm) are likely due to the orbit calculation differences between both missions. The ageing of Jason-1 (no more GPS data) explains very likely these differences.

Then, additional Jason-2 cycles will not be useful to better analyze the Jason-2 SSH performances and the SLA consistency with Jason-1. From this Cal/Val point of view, and in order to better benefit from these both missions for scientific applications, Jason-1 satellite can then be moved to its new interleaved orbit as soon as possible.

CLS Collecte Localisation Satellites
8-10 rue Hermes
31520 Ramonville Saint-Agne - France

OSTST
Nice, November 2008

Figure 63: *Poster presented at OSTST meeting, Nice 2008*

Assessment of Jason-2 and Jason-1 orbit quality from SSH analysis

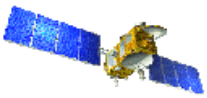

M. Ablain[1], I.Pujol[1],S. Philipps[1], N.Picot[2]

[1]CLS, Space Oceanography Division, Toulouse, France
[2]CNES, Centre National d'Études Spatiales, Toulouse, France

Overview

The OSTM/Jason-2 satellite was successfully launched on 20th of June, 2008. Since 4th of July Jason-2 is on the same orbit as Jason-1 spaced out by 55 seconds. The Cal/Val phase allows us to check very accurately the Sea Surface Height (SSH) consistency provided by both satellites. Actually, as the altimeter parameter consistency between both missions seems very good, the Jason-1/Jason-2 SSH cross-calibration directly provides an estimation of the quality of the orbit underlining eventual geographically correlated biases, jumps or drifts. The objectives of this study is then to present the quality of Jason-2 and Jason-1 orbits (DIODE, MOE and preliminary POE orbits) through the SSH calculation. Along-track and crossover analyses are performed from the beginning of the mission to compare the system performances using the different orbits in the SSH calculation provided by Jason-1 and Jason-2. Cross-calibration with Envisat data is also performed to complete these analyses.

Along track SLA analyses / Comparisons with Jason-1

Jason-1 and Jason-2 SLA differences are mapped over all the Jason-2 period using successively MOE orbits (from IGDRs) from cycles 1 to 10 and POE orbit provided by CNES and GSFC from cycles 1 to 7. Jason-2 POE orbits are preliminary since Jason-2 GDRs are not yet available. Note that no correction is applied to the SLA calculation (only Orbit - Range - MSS) since both altimeters are spaced out by 55s.

Mean of J1/J2 SLA differences (cm)

SLA differences with CNES MOE orbits (fig.1) highlight large correlated geographically biases within +/-3 cm in average. These biases vary in space and time (for each cycle) and they can reach +/- 5 cm.

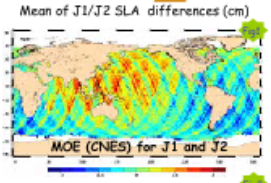

Using CNES POE orbit, Jason-1/Jason-2 SLA consistency (fig.2) are dramatically improved. However, weak hemispheric differences remain close to 1 cm. In addition, this correlated geographically bias is stable in space and time.

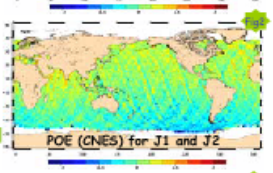

Replacing CNES POE orbit by GSFC orbit only for Jason-2 SLA has no impact on Jason-1/Jason-2 SLA consistency (fig.3) : the weak hemispheric differences are still observed.

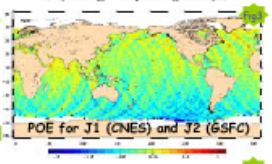

Finally, using GSFC POE orbits provided for both missions, allows us to obtain a more homogenous map. SLA differences are now lower than 0.5 cm and do not show any specific structures (fig.4).

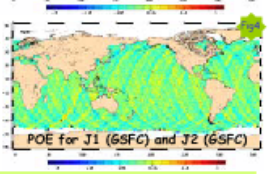

This analysis shows the great impact of the orbit calculation on the SLA consistency between Jason-1 and Jason-2. It highlights that the small residual differences observed on SLA consistencies (with POE) are mainly due to the orbit calculation. However it does not allow us to determine which is the best orbit solution.

Cross-Calibration with Envisat

Using MOE orbit, the SLA consistency is better between Jason-2 and Envisat than between Jason-1 and Envisat.

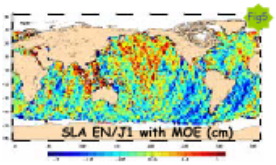

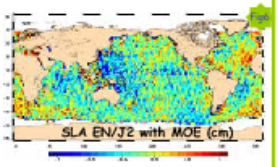

Cross-calibration with Envisat measurements is also performed to check the SLA consistency with Jason-1 and Jason-2. But in this case, both Jason satellites do not measure the same SSH at the same time. Then it is mandatory to cumulate SLA differences over a long enough period to average the oceanic variability discrepancies. Then, we focus here our analysis on SLA differences calculated with MOE orbits, since 11 Jason-2 cycles are available.

SLA consistency is better between Jason-2 and Envisat than with Jason-1 (fig.5 and 6). Correlated geographically biases observed from Envisat/Jason-1 (fig.5) are very well correlated with those detected from Jason-1/Jason-2 (fig.1). This brings out the good consistency of Jason-2 and Envisat MOE orbit. This may indicate also that Jason-1 MOE could be refined.

SSH Crossovers analyses / Comparisons with Jason-1

The monitoring of Jason-1 and Jason-2 SSH statistics at crossovers are performed using successively DIODE, MOE and POE orbits, allowing us to compare the relative performances of each orbit. Thanks to the new Jason-2 DIODE orbit, a dramatic improvement is observed: mean of SSH crossover are more stable and better centered than Jason-1 (fig.2) and standard deviation are significantly lower (fig.4).
Concerning MOE and POE orbits, similar statistics are plotted (fig.1 and 3). A slightly improvement is observed using Jason-2 MOE in comparison with Jason-1 especially for the standard deviation (5.5 cm RMS for J2 instead 5.7 cm RMS for J1 (fig.3)). Results is reversed comparing the GDRs products, but the CNES Jason-2 's POE orbit is preliminary at the moment.

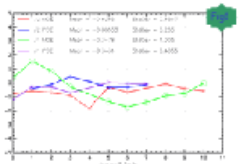

Mean of SSH crossovers (cm)

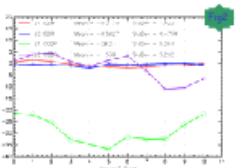

Impact of MOE and POE orbits for J1 and J2

Impact of DIODE orbits for J1 and J2

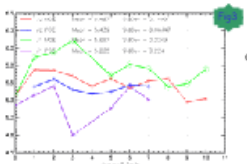

Standard deviation of SSH crossovers (cm)

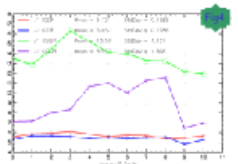

Performances of New GDR-C Jason-1 orbit over all the Jason-1 period

GDR-C orbit is a SLR/DORIS/GPS orbit as GDR-B but uses the EIGEN-GL04C gravity field, taking into account annual and semi-annual time variability, atmospheric contribution of the gravity field and ocean pole tide effects. In addition, the new reference frame used is ITRF2005.

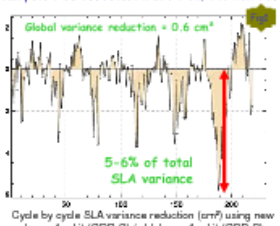

Cycle by cycle SLA variance reduction (cm²) using new Jason-1 orbit (GDR-C) / old Jason-1 orbit (GDR-B)

Mean differences at crossovers are more homogeneous geographically, proving a better coherence with version C (not shown here). A stronger improvement is observed from along-track analyses. Indeed, the SLA variance difference using successively GDR-C and GDR-B POE orbits highlights an annual signal (fig.1) with a strong reduction of variance (until 6 cm²). This feature has also been observed when comparing the altimetry to in situ measurements (Tide gauges and ARGO T/S profiles).

The impact of new GDR-C orbit on global MSL trend is weak (< 0.1 mm/yr). But hemispheric regional trends are impacted by the new ITRF2005 solution within +/-2 mm/yr (fig.2). Hemispheric MSL trend differences are now more homogenous (1.94 mm/yr slope difference with GDR-B orbit instead of 1.40 mm/yr with GDR-C orbit). However, the impact on hemispheric MSL trends is weaker compared to the GSFC ITRF2005 orbit (see Ablain's poster : Error estimation of the global and regional mean sea level trends).

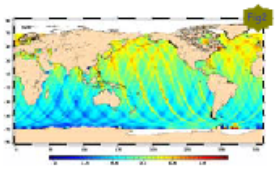

Regional MSL trend differences (mm/yr) using new Jason-1 orbit (GDR-C) / old Jason-1 orbit (GDR-B)

Conclusion

This study aims at underlining the very good quality of Jason-2 orbits. It's especially true for the DIODE orbit which dramatically improves SSH statistics at crossovers in comparisons with Jason-1. Though, MOE and POE orbits show similar performances for both satellites at crossovers, the analysis of SLA consistency highlights a better coherence between Jason-2 and Envisat MOE than with Jason-1 MOE. These not negligible differences (+/- 5 cm) , probably due to the Jason-1 MOE calculation impact directly the quality of multi-mission products using Jason-1 as the main altimeter mission (DUACS product for instance). Finally, the SLA consistency analysis using different POE orbits (CNES, GSFC) is in a good agreement (+/- 1 cm). However it also shows that the POE orbit calculation remains the main source of SLA discrepancies between Jason-1 and Jason-2.

CLS Collecte Localisation Satellites
8-10 rue Hermes
31520 Ramonville Saint-Agne - France

OSTST Nice, November 2008

cnes

Figure 64: *Poster presented at OSTST meeting, Nice 2008*